Charles University in Prague
Faculty of Mathematics and Physics

DIPLOMA THESIS

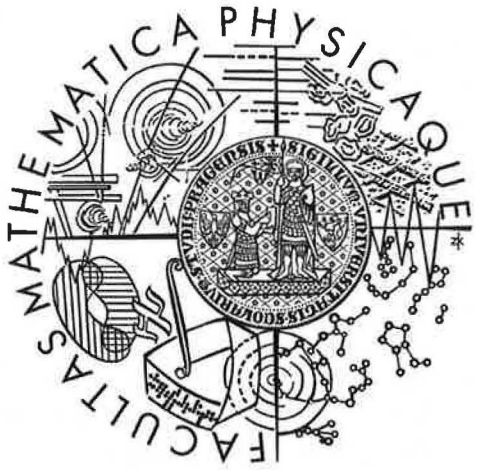

Bc. Dana Turčinková

Pressure influence on magnetic parameters of intermetallic compound

Department of Condensed Matter Physics

Supervisor: Prof. RNDr. Vladimír Sechovský, DrSc.

Study program: Physics, Physics of Condensed Matter and Materials

2009

In the place, I would like to express my aknowledment to everyone who helped me during my diploma study and who contributed to finish this thesis.

First of all, I would like to thank to my supervisor, prof. RNDr. Vladimír Sechovský, DrSc. for his patient leading all the time of my diploma study, for his leanguage and technical corrections and valueable advices in discussion about the explored problematic and obtained results.
I am very thankful to Mgr. Matuš Mihálik, Ph.D. for his patient help in my experimental beginnings.
I would like to thank to Mgr. Jiří Pospíšil for his introduction into samples' preparation, characterization and modification, his explanation of related issues and mainly for his help with the final samples' preparation.
I would like to thank to Mgr. Klára Uhlířová for her help with sample's characterization and modification.
I am thankful to RNDr. Eva Šantavá and Ing. Josef Šebek, PhD. who introduced me into instruments' control and helped me with progression of the experiments.
I am very grateful to Bc. Roman Havlíček for his help with diffraction-data analysis.
I would like to thank to RNDr. Jan Prokleška, Ph.D. for his help with experiments in Closed Cycle Refrigerator and for discussions about insturments' principles and $RECo_2$ systems.
I would like to thank to doc. RNDr. Martin Diviš, CSc for his remarks to the theoretical part of this thesis.
I would like to thank to Dr. Jiří Kamarád for his help with uniaxial-pressure experiments, his explainations of pressure-cell principles and his discussion about obtained results.
I would like to thank to RNDr. Jiří Prchal, Ph.D. and Mgr. Martin Míšek who taught me how to prepare hydrotatic-pressure experiments, I am very thankful for their help with progressions of the experiments and for their valuable advice and discussions.

At the end, I would like to thank to my Laurent for his patience and also help with Word- and Origin-programs and mainly to my parents who always supported in everthing I was doing and allowed my to study.

Prohlašuji, že jsem svou diplomovou práci napsala samostatně a výhradně s použitím citovaných pramenů. Souhlasím se zapůjčováním práce.

Contents

Contents 4

Chapter 1 Introduction 8

Chapter 2 Theory 9
2.1 Magnetism 9
2.1.1 Localized electron model of magnetism 9
2.1.2 Itinerant electron model of magnetism 13
2.1.3 Magnetic order 14
2.2 Electrical transport 15
2.2.1 Electrical resistivity 15
2.2.2 Magnetic field influence 16
2.3 External pressure and its influence 16
2.3.1 Basic definitions 17
2.3.2 Pressure influence 17

Chapter 3 Previous results on studied materials in literature and motivations of this thesis 19
3.1 Cubic Laves phase structure 19
3.2 $ErAl_2$ compound 19
3.3 $RECo_2$ (RE = rear earth atom) compounds 20
3.3.1 $RECo_2$ compounds and itinerant electron metamagnetism 20
3.3.2 Composition of $RECo_2$ 21
3.3.3 Electronic and magnetic properties of the $RECo_2$ compounds with special interest in $ErCo_2$ 21
3.3.4 Theoretical background 22
3.3.5 Parrimagnetism 23

Chapter 4 Experimental methods applied 26
4.1 Sample preparation 26
4.2 Sample characterization 26
4.2.1 X-ray powder diffraction 26
4.2.2 Microprobe analysis 26
4.3 Bulk investigation techniques 27
4.3.1 Magnetization measurements 27
4.3.2 Electric resistivity measurements 28
4.4 Pressure techniques 29
4.4.1 Hydrostatic clamp pressure cells 29
4.4.3 Diamond anvil cells 31
4.4.2 Uniaxial pressure cell 32

Chapter 5 Properties of $ErAl_2$ compound 34
5.1 Results and discussion 34
5.1.1 Magnetic properties at ambient pressure 34

5.1.2 Magnetic properties under hydrostatic pressure 34
5.1.3 Magnetic properties under uniaxial pressure 35

Chapter 6 Properties of $Er(Co_{1-x}Si_x)_2$ compounds with x = 0, 0.25 36
6.1 Results and discussion 36
6.1.1 Structure and composition analysis 36
6.1.2 Magnetization behaviour 37
6.1.4 AC susceptibility behaviour 41
6.1.2 Electrical resistivity behaviour 47
6.2 Conclusions 51

Appendix A 53

Reference 54

Název práce: Vliv tlaku na magnetické parametry intermetalické sloučeniny
Autor: Bc. Dana Turčinková
Katedra: Katedra fyziky kondenzovaných látek
Vedoucí diplomové práce: prof. RNDr. Vladimír Sechovský, DrSc.
Email vedoucího: sech@mag.mff.cuni.cz
Abstrakt: Tato práce pojednává o magnetických a elektrických vlastnostech sloučenin $ErAl_2$, $ErCo_2$ and $Er(Co_{0.975}Si_{0.025})_2$ v atmosférickém, hydrostatickém nebo jednoosém tlaku. Výsledky pro $ErAl_2$ potvrdily odlišný vliv působení hydrostatického a jednoosého tlaku na magnetický moment a AC susceptibilitu. Pro $ErCo_2$ and $Er(Co_{0.975}Si_{0.025})_2$ byly provedeny detailní studie teploty přechodu T_C, flipping-teploty T_F a magnetického momentu. Bylo pozorováno, že $ErCo_2$ vykazuje silnou nestabilitu magnetism v Co podmříži spojenou s výraznými spinovými fluktuacemi, které se projevují v silném navýšení elektrického odporu v okolí nad T_C a vedoucí dokonce k rozštěpení T_C pod dostatečně vysokým tlakem. Substituce křemíku za Co vede ke stabilizaci Co magnetismu. Z výzkumů T_F bylo usouzeno, že původ parimagnetismu je určen především výměnnými interakcemi v kobaltové podmříži.
Klíčová slova: itinerantní elektronový magnetismus, $ErCo_2$, vliv tlaku, spinové fluktuace.

Title: Pressure influence on magnetic parameters of intermetallic compound
Author: Bc. Dana Turčinková
Departement: Departement of Condensed Matter Physics
Supervisor: prof. RNDr. Vladimír Sechovský, DrSc.
Supervisor's e-mail address: sech@mag.mff.cuni.cz
Abstract: This thesis deals with magnetic and electronic properties of the $ErAl_2$, $ErCo_2$ and $Er(Co_{0.975}Si_{0.025})_2$ compounds at ambient, hydrostatic or uniaxial pressure. The results for $ErAl_2$ confirmed different influence of hydrostatic and uniaxial pressure on the Er-magnetic moment and AC susceptibility. As for $ErCo_2$ and $Er(Co_{0.975}Si_{0.025})_2$, detailed studies of the transition temperature T_C, flipping temperature T_F and magnetic moment were performed. It was observed that the $ErCo_2$ proves strong instability of Co magnetism accompanied by strong spin fluctuations demonstrated as strong enhancement of the near-above-T_C anomaly and leading even to splitting of the T_C under applied pressure. The substitution of Si for Co causes stabilization of magnetism in the Co sublattice system. From investigations of the T_F, it was concluded that origination of parimagnetism is driven mainly by interactions in the Co sublattice.
Keywords: itinerant electron magnetism, $ErCo_2$, pressure influence, spin fluctuations.

Chapter 1 Introduction

The large family of the RE-T (RE = rare earth atoms, T = Mn, Fe, Co, Ni) compounds have been for many years matter of special interest because of offering possibilities to study various aspects of transition-metal magnetism. While the behaviour of the compounds containing Mn, Fe and Ni is more or less explained, the behaviour of materials with Co proves still new features. The $RECo_2$ family serves good examples of broad variety magnetism of the Co sublattice under different conditions. Studies are frequently concentrated in various aspects of itinerant electron magnetism.
The $ErCo_2$ compound is especially very interesting because the Co sublattice appears on the verge of magnetism. A number of experimental and theoretical works was done and one could think that the picture of this system is already complete but recently a new phenomenon concerning the existence of Co-magnetism in paramagnetic state has been discovered. The discovery and description of *paramagnetism* brought a now momentum in the research of $RECo_2$ compounds, which was also the primary motivation of this thesis.
The envisaged task of the thesis was determination of dependence of the characteristic temperature of parimagnetism T_F (flipping temperature) on the substitution of Si for Co and on applied hydrostatic pressure by measuring the AC susceptibility in a SQUID magnetometer using the available pressure cell operating in moderate pressures. Sample preparation and characterization was done in the technology, X-ray laboratories of the Department of Condensed Matter Physics (DCMP) and in the joint microscopy laboratory of DCMP and the Department of Plasma and Surface Science. The entire experiments were performed in the Joint Laboratory for Magnetic Studies (JLMS) conducted by DCMP. The recent development of pressure cells in JLMS allowed extending the experiments far beyond the envisaged tasks owing to measurements of magnetization, AC susceptibility and electrical resistivity up to much higher pressures than originally intended. Besides determining the alloying and pressure effects on T_F further important information concerning physics of $ErCo_2$ has been obtained and some interpretation of new features has been proposed. In addition a comparative study of the dependence of the magnetic ordering temperature and the Er magnetic moment on hydrostatic and uniaxial pressure has been pursued.

The outline of this thesis is organized as the following: **Chapter 1** gives the general introduction of this thesis, in **Chapter 2** general aspects of magnetism of localized- and itinerant-electron system are described together with concepts concerning the influence of external pressure on magnetic phenomena. **Chapter 3** resumes important findings about $ErAl_2$ and $ErCo_2$ which point to the motivation of our work. **Chapter 4** presents the experimental techniques and instruments that were used for the magnetic and electrical measurements at ambient and under hydrostatic and uniaxial pressure. In **Chapter 5** the results from magnetic measurements of $ErAl_2$ single crystal under hydrostatic and uniaxial pressure are presented and discussed. **Chapter 6** is concerned with all the experiments on the $ErCo_2$ and $Er(Co_{0.975}Si_{0.025})_2$ polycrystalline samples. Employing magnetic and electric measurements at ambient and hydrostatic pressure, we try to give explanation about process taking place and improve knowledge about the complex magnetic system.

Chapter 2 Theory

2.1 Magnetism

In magnetic measurements, we are interested in behaviour of the magnetic moments of the studied material with or without applied magnetic field. The measured quantity is usually the magnetization (magnetic dipole moment per unit volume), from which the magnetic susceptibility can be calculated as a response of the magnetization on the change of an applied magnetic field.
Existence of stable magnetic moments is expected in ions of transition elements that have partially occupied the *d*- or *f*-electron energy states. The magnetic moments of a free transition-element ion can be straightforward calculated within the quantum mechanical model. When such an ion appears embedded in condensed matter its "magnetic" electrons are exposed to various interactions with electrons of neighbouring ions that can modify the electron wave functions and hence the magnetic moments. The exchange interactions also correlate magnetic moments of neighbouring ions. Frequently this yields a very complex situation in a real material that is not easy to treat theoretically.

In this thesis we handle intermetallics that are composed of rare-earth lanthanide atoms and transition-metal atoms. For fully detailed understanding of their magnetic properties complicated theoretical calculation would be necessary, but sometimes already simple approximations can lead to qualitative clarification.
Two extreme limits find reasonable theoretical description, magnetism of localized electros on one side and magnetism of itinerant electrons on the other. The first case matches well behaviour of most of lanthanide ions in any chemical environment because their 4f-electron wave functions are well shielded from surrounding and so a crystal containing rare-earth ions can be treated in first approximation as a collection of free ions with perturbations caused by the interactions with ligand surroundings (crystal-field effects) or by the interactions with each other (exchange interactions). On the other hand, the much extended *d*-electron wave functions in metals and intermetallics yield a strong delocalisation of *d*-electrons and band theory finds better description in these materials.

2.1.1 Localized electron model of magnetism

This part was worked out with the help of following literature: Ashcroft and Mermin [1]; Blundell [2].

Magnetism of free atoms and ions

The magnetic moment on an atom is associated with the total angular momentum *J*. The actual composition of the *J* depends on coupling between the orbital and spin angular moments of the electrons (spin-orbit coupling). For most of the elements, the *L*-*S* coupling, also known as Russell-Saunders coupling, holds. This means that the spin-orbit interaction is a weak perturbation and the main energy terms are determined by the electrostatic interactions that control the values of *L* and *S*, i.e. by combining separately the orbital and spin angular moments for the electrons. For very heavy atoms (i.e. heavy actinide atoms), the

spin-orbit interaction dominates and the spin and orbital angular momentum of each electron are coupled separately. Then the weaker electrostatic interaction may couple the total angular momentum of each electron (j), which is called the j-j coupling. Further, we will consider only the L-S coupling here.

There is a large number of possible superpositions of angular- and spin-momentum quantum numbers but only one minimizes the energy and yields the ground state for a particular ion. This can be described by a set of the Hund´s rules:

1. The state that has the lowest energy has the largest total spin S, which is consistent with the Pauli Exclusion Principle.

2. Among the states with the same value of S, the state with the largest total orbital angular momentum L has the lowest energy.

3. With the satisfaction of the previous two rules, the value of the total angular momentum J corresponding to the state of the lowest energy is:

$$\begin{aligned} J &= |L - S| \quad \text{for } n \le (2l+1), \\ J &= L + S \quad \text{for } n \ge (2l+1). \end{aligned} \tag{2.1}$$

From the thermodynamic theory the susceptibility is defined as:

$$\chi = \frac{\partial M}{\partial H} = -\frac{1}{V}\frac{\partial^2 F}{\partial H^2} = -\frac{1}{V}\frac{\partial^2 \Delta E}{\partial H^2}, \tag{2.2}$$

where F is the magnetic Helmholtz free energy and ΔE is an energy shift (obtained from the second-order perturbation theory) defined as:

$$e^{-\beta F} = \sum_n e^{-\beta E_n(H)} \qquad ;\beta = 1/k_B T \tag{2.3}$$

$$\begin{aligned} \Delta E_n = \mu_B \hat{H} \cdot \left\langle n \middle| \hat{L} + g_0 \hat{S} \middle| n \right\rangle + \sum_{n \neq n'} \frac{\left| \left\langle n \middle| \mu_B \hat{H} \cdot \left(\hat{L} + g_0 \hat{S} \right) \middle| n' \right\rangle \right|^2}{E_n - E_{n'}} \\ + \frac{e^2}{8mc^2} H^2 \left\langle n \middle| \sum_i \left(x_i^2 + y_i^2 \right) \middle| n \right\rangle \end{aligned} \tag{2.4}$$

Depending on the shell structure of an ion and on the following total orbital and spin angular momentum one gets the atomic susceptibility of a solid composed of N such ions.

(i) The last term from the Eq. 2.4 is independent on S and L and yields the negative Larmour diamagnetic susceptibility of closed (fully occupied electron states) electron shells (characterized by $S = 0$, $L = 0$) of any ion or atom (inner shells):

$$\chi_{dia} = -\frac{e^2}{6mc^2}\frac{N}{V}\left\langle 0 \middle| \sum_i r_i^2 \middle| 0 \right\rangle. \tag{2.5}$$

If electron states within outer shell are not fully occupied L or S are nonzero and the first and

the second term of the Eq. 2.4 plays an important role.

(ii) In the case of an ion or atom with the shells that are one electron short of being half filled the ground state $J = 0$ (while $L = S \neq 0$) and consequently second term of the Eq. 2.4 is zero and the susceptibility is given as:

$$\chi = -\frac{N}{V}\left[2\mu_B^2 \sum_n \frac{\left|\langle 0|\left(\hat{L}_z + g_0 \hat{S}_z\right)|n\rangle\right|^2}{E_n - E_0} + \chi_{dia} \right] \tag{2.6}$$

The first term of this equation is the paramagnetic (positive susceptibility), temperature independent, Van Vleck term.

(iii) Generally, if $J \neq 0$ the ground state is $(2J+1)$-fold degenerate in zero field. If only $2J+1$ states are thermally excited with appreciable probability then the free energy is given by:

$$e^{-\beta F} = \sum_{J_z=-J}^{J} e^{-\beta\gamma H J_z} \quad ; \gamma = g(JLS)\mu_B \tag{2.7}$$

The magnetization corresponding to the second term in the Eq. 2.4 is now nonzero and temperature dependent and given as:

$$M = -\frac{N}{V}\frac{\partial F}{\partial H} = \frac{N}{V}\gamma J B_J(\beta\gamma J H), \tag{2.8}$$

where $B_J(x)$ is Brillouin function that is defined as:

$$B_J(x) = \frac{2J+1}{2J}\coth\frac{2J+1}{2J}x - \frac{1}{2J}\coth\frac{1}{2J}x \tag{2.9}$$

For $\gamma H << k_B T$ (using the small x-expansion in $B_J(x)$ for $x << 1$) we obtain for the susceptibility so called Curie law:

$$\chi = \frac{N}{3V}\frac{\mu_B^2 \mu_{eff}^2}{k_B T} \tag{2.10}$$

Crystal field effects

The electrostatic potential of an ion in a solid is in general different than the one of a free ion. The charge distribution of the ion environment causes an electrical field with symmetry of the environment. Interaction of a localized electron with the field due to surrounding atoms or ions is called the crystal field interaction.
The total energy of the system is given by the Hamiltonian:

$$H = H_0 + H_{SO} + H_{CF}, \tag{2.11}$$

where H_0 is the unperturbed energy of free ion, H_{SO} is the spin-orbit coupling term and H_{CF} is the crystal field term.

(i) In the transition metals, the $3d$ shells are the outermost ones and the crystal field is much larger than spin-orbit coupling. Hund's rules determine the ground state values of L and S and the crystal field is the largest perturbation.

(ii) In the case of rare-earth metals, the $4f$ moments are well shielded by the full $5s$- and $5d$-shells. The crystal field is much weaker than the spin-orbit coupling and can be considered as a perturbation. Owing to this fact, it is usually sufficient for magnetic properties to consider only the lowest multiplet J (given by Hund's rules) which degeneracy is completely or partial lifted. In some cases can occur, if J is integer, that the ground state has $J_z = 0$ and the ground state is then non-magnetic.
The crystal-field Hamiltonian can be written as:

$$H_{CF} = \sum_m \sum_n A_n^m \sum_i f_{nm}(r_i), \tag{2.12}$$

where f_{nm} are operators derived from Tesseral harmonics describing the spatial distribution of the charge associated with the $4f$ electrons, A_{nm} describes the spatial distribution of the charge surrounding the $4f$ electrons.

Interactions

Until now we assumed free ions i.e. discrete carriers of magnetic moments that do not interact with each other. But if there were no interactions then, in the absence of a field, the individual magnetic moments would be thermally disordered, would point in random directions, could not sum to a net moment and finally, no long-range order would be observed. Generally, there are two types of interactions that yield correlations of pairs of magnetic moments - the magnetic dipolar interaction and the exchange interaction. The magnetic dipolar interaction is very weak and therefore becomes important only at very low temperature region. It cannot serve for the explanation of the ordering in the most magnetic materials.

The exchange interactions are usually treated by the Heisenberg model where exchange interaction between two ions is expressed by the spin Hamiltonian. The total spin Hamiltonian of the system summed over all pairs of ions is then given as

$$\hat{H} = -\sum_{ij} J_{ij} \hat{S}_i \cdot \hat{S}_j \tag{2.13}$$

where J_{ij} is the exchange constant (or exchange integral) between two spins $\hat{S}_i$ and $\hat{S}_j$.

There are three basic types of the magnetic exchange interactions, which can be responsible for creation of magnetic ordered state:

(i) *Direct exchange*. The direct exchange arises from the direct Coulomb interactions among electrons from two ions. This type of interactions typically occurs in compounds with d-electron ions in magnetic state because the d-electron orbitals of neighbouring atoms are considerably overlapped. This interaction is strong but short-range and it is responsible for high ordering temperatures but usually small magnetic moments.

(ii) *Indirect exchange – superexhange.* This interaction is typical for materials in which the magnetic ions are separated by non-magnetic ions. In this case, the interaction is mediated via polarization of ligand state of nonmagnetic ions (Blundell [2]). It arises typically in transition-metal oxides (Lacroix [3]).

(iii) *Indirect exchange in metals – mediated by conduction electrons - RKKY interaction.* This interaction arises in metallic systems when magnetic moments remain localized, as in the rare-earth metals or rare-earth intermetallics. It is caused by the localized magnetic moment that spin-polarizes the conduction electrons in its neighbourhood and the spin polarization propagates to other magnetic ions within range, leading to an indirect coupling. The interaction is long-range and has an oscillatory dependence on the distance between magnetic moments. Therefore, depending on the separation between two ions, the magnetic coupling may be either ferromagnetic or antiferromagnetic.

2.1.2 Itinerant electron model of magnetism

Until now the localized model of magnetism was sufficient as we supposed that band character of the electrons could be neglected. At this moment we will describe the other extreme limit of magnetism as we will deal with delocalised (itinerant) band electrons which properties are described by a new quantum number, the electron momentum k (Mohn [4]). These electrons participate either on magnetic or on transport properties. In such a system, spontaneously spin-split bands is responsible for the magnetic ordering that is characterized by a non-integer value of the atomic moments. Typical examples are the 3*d* metals Fe, Co and Ni.

Stoner model

One simple model for itinerant magnetism is the Stoner model (e.g. Lacroix [3]; Mohn [4]; Givord [5]; Bushow [6]; Gignoux et al. [7]) (based on the fact that the carriers of magnetism are the electrons in the d band [4])) in which the electrons are assumed to be fully delocalised characterized by an electronic band structure. The exchange interactions between itinerant electrons are given as

$$E_M = U\, n_\uparrow\, n_\downarrow , \tag{2.14}$$

where $n_\uparrow$ and $n_\downarrow$ are the number of electrons for each spin state and U is the on-site Coulomb repulsion between electrons of opposite spins that tends to increase the number of electrons with spin up. Suppose an infinitesimal transfer of electrons from minority to majority band – the magnetic state of the system is now dependent whether this becomes energetically stable. By this process, energy is gained due to the magnetic contribution ΔE_M to the variation of electron energy and lost due to the occupation of states of higher kinetic energies ΔE_K. The total change of energy ΔE is given as

$$\Delta E = \Delta E_M + \Delta E_K = \left[(n^2 m^2)/4N(E_F)\right]\left[1 - U\,N(E_F)\right] \tag{2.15}$$

where $n = n_\uparrow + n_\downarrow$, $m = (n_\uparrow - n_\downarrow)/n$ and $N(E_F)$ is the density of states at the Fermi level per spin in the paramagnetic state – ferromagnetism is thus favoured by a high density of states at the Fermi level.
Ferromagnetism is obtained when the exchange field splits the spin subband - an infinitesimal transfer of electron from minority to majority bands becomes energetically stable. This is given by the Stoner criterion $U\,N(E_F) \geq 1$.

Actually, according to the Stoner criterion one can distinguish more special cases of magnetic materials when the Stoner product:

(i) $U\,N(E_F) < 1$ … the Pauli paramagnetism is observed in applied field,

(ii) $U\,N(E_F) <$ and $\cong 1$ … the compound is close to the onset of ferromagnetism and may exhibit the collective electron metamagnetism (Wohlfarth et al [8]),

(iii) $U\,N(E_F) > 1$ … the Stoner criterion is fulfilled but magnetization is small; in this case majority carrier (spin up electrons) bands are not completely filled, minority bands are often empty (Mohn [4]); such systems are called the weak itinerant ferromagnets,

(iv) $U\,N(E_F) > 1$ ... the majority bands are completely filled and the minority bands are partially filled; these compounds are called the strong itinerant ferromagnets.

Even in the case that the Stoner product is still small to achieve a ferromagnetic state there can be still observed a considerable enhancement of the magnetic susceptibility due to the positive exchange interaction of the band electrons (Ibach and Luth [9]). The exchange enhanced susceptibility at $T = 0$K and in a field H is given as (e.g. Bushow [6])

$$\chi = \frac{\chi_0}{1 - U\,N(E_F)}\ , \tag{2.16}$$

where χ_0 is the Pauli susceptibility[1] and $1/[1-U.N(E_F)]$ is called Stoner enhancement factor.

In the framework of the Landau theory of phase transitions (where the bulk magnetic moment is introduced as the order parameter for the free energy), the temperature dependence of magnetic moment and susceptibility can be derived but the inverse susceptibility shows T^2-behaviour (Mohn [4]).

Spin fluctuations model

The simplifying Stoner model is quite successful when describing an itinerant system in its ground state but there are disagreements between predicted behaviour and experimental data for finite temperatures, mainly in the values of Curie temperature or the temperature dependence of susceptibility (Mohn and Khmelevskyi [10]). An improvement has been achieved by introducing thermally induced collective excitations by Moriya [11] and later involving fluctuations of the spin density (spin fluctuations) by Murata and Doniach [12] into the systems. Especially, when leaving the Landau theory the original order parameter M should be replaced by a new quantity containing the fluctuating magnetic moment also. The consequence for the paramagnetic state is that owing to the fluctuations the thermally induced local magnetic moments are present even without bulk magnetization.

2.1.3 Magnetic order

If in the solid is some of the type of magnetic interaction mentioned above the solid will reach ordered state under condition that the magnetic interaction is stronger than thermal fluctuations. There are several types of magnetic ground state including ferromagnetism, ferrimagnetism, antiferromagnetism, spiral and helical structures or spin glasses etc. It is given a short description of orders that proves materials studied by us.

[1] Is the susceptibility in metallic system of non-interacting (no exchange) gas of free electrons given as $\chi_0 = 2\mu_B^2.N(E_F)$.

Ferromagnetism
A ferromagnetic system proves a nonzero magnetic moment even in the absence of applied magnetic field (=spontaneous magnetization). The total field experienced by the magnetic moments is given by the applied field and the molecular field (or Weiss field)

$$\vec{H}_{tot} = \vec{H} + \vec{H}_m = \vec{H} + \lambda M , \tag{2.17}$$

where λ is the Weiss-field coefficient, which parameterizes the strength of the molecular field and which is $\lambda > 0$ for ferromagnets.
Under the ordering temperature, called Curie temperature T_C, all the individual moments are aligned parallel to each other. In the paramagnetic state, the susceptibility of the material follows the Curie-Weiss law

$$\chi = \frac{C}{T - \theta_P}, \quad C = \frac{N_A \mu_{eff}^2}{3k_B} \tag{2.18}$$

where C is the Curie constant, θ_P is the paramagnetic Curie temperature, N_A si the Avogadro's number and μ_{eff} is the effective moment. In a ferromagnet, $\theta_P = T_C > 0$

Ferrimagnetism
In a ferrimagnetic system, two sublattices A and B with different absolute values of corresponding magnetic moments are present. In the ordered state, moments of in the frame of each sublattice are aligned ferromagnetically and the two sublattices are aligned antiparallel to each other proving a spontaneous magnetization.
Above the T_C, the paramagnetic inverse susceptibility is given as

$$\chi^{-1} = \frac{T}{C} - \chi_0^{-1}, \quad \chi_0^{-1} = \frac{1}{C^2}\left(C_A^2 \lambda_A + C_B^2 \lambda_B + 2C_A C_B \lambda_{AB}\right), \tag{2.19}$$

where λ_A, λ_B and λ_{AB} and intra- and inter-sublalttice exchange coeffiecients.

2.2 Electrical transport

2.2.1 Electrical resistivity

The electrical resistivity of a material is a consequence of the scattering of the conduction electrons on different scattering-centres. In accordance to the Matthiessen's rule (e.g. Singleton [13]), the different scattering-processes can be treated as independent of each other. Consequently, the resistivity of a material is given as a sum of the particular contributions (Ibach and Luth [9]). The main contributors are the temperature independent residual resistivity, the resistivity given by scattering on the phonons and in the case of magnetic materials the resistance caused by the spin-dependent scattering of conduction electrons on magnetic carriers.

$$\rho(T) = \rho_0 + \rho_{ph}(T) + \rho_{mag}(T) \tag{2.20}$$

Residual resistivity

The residual resistivity is caused by the electron scattering occurring on dislocations, point defects and grain boundaries. These processes are elastic, so no energy transfer between the conduction-electron system and the scatterer appears. Scattering on defects is temperature independent.

Phonon scattering

At room temperature, the electron scattering on phonons contributes mostly to the total resistance. Using the Debay model describing the lattice dynamics, the contribution is given by Bloch-Grüneisen formula:

$$\rho_{ph} = 4C_{ph}\left(\frac{T}{\theta_D}\right)^5 \int_0^{\theta_D/T} dx \frac{x^5}{(e^x - 1)(1 - e^{-x})}, \tag{2.21}$$

where C_{ph} is an additional parameter and θ_D is Debye temperature. In the boarding cases of high and low temperatures, respectively, holds:

$$\begin{aligned} &\rho_{ph}(T) \propto T \quad \text{for } T >> \theta_D . \\ &\rho_{ph}(T) \propto T^5 \quad \text{for } T << \theta_D , \end{aligned} \tag{2.22}$$

Spin-dependent scattering

The electrical resistivity depends on whether the material is in a magnetically ordered state or not. In the paramagnetic state, the magnetic moments are disordered and the contribution to the electrical resistivity is temperature independent if we neglect the crystal field, short-range ordering and spin-spin correlations effects. The spin-dependent scattering of conduction electrons becomes strongly reduced in a ferromagnetic state.

2.2.2 Magnetic field influence

Suppose now, electrons being now affected both by external electric and magnetic field. By application of an external magnetic field the conduction electron does not get any additional drift velocity just their trajectories and also the charge current are influenced.
The resistivity should be treated as a tensor that is simplified in the case of material with cubic symmetry and field applied in z-direction as followed:

$$\ddot{\rho}(\vec{B}) = \begin{pmatrix} \rho_\perp(B) & \rho_H(B) & 0 \\ -\rho_H(B) & \rho_\perp(B) & 0 \\ 0 & 0 & \rho_{||}(B) \end{pmatrix}, \tag{2.23}$$

where $\rho\perp$ and $\rho_{||}$ are resistivities in perpendicular and parallel direction of magnetic field to electric current and ρ_H is the Hall resistivity.

2.3 External pressure and its influence

Interatomic distances play the key role in interactions responsible for magnetism in solids. The application of a pressure enables to vary them and study the resulted consequences without occurring any accompanying effect as by chemical substitutions (called sometimes also "chemical pressure"). The high-pressure experiments are so a valuable tool for obtaining the information about the electronic structure and the magnetic character of a material.

2.3.1 Basic definitions

Mechanical straining of a body can be described in Cartesian system x_i ($i = 1, 2, 3$) by a stress tensor σ_{ij} with six independent components ($\sigma_{ij} = \sigma_{ji}$) (Kamarád [14]). Surface stresses acting on an internal plane are typically decomposed into three orthogonal components. One component is normal to the stressed surface and represents direct stress (σ_{ii}) that tends to change the volume of a body, the other two components are parallel to the stressed surface and represent shear stresses (σ_{ij}, $i \neq j$) that tend to deform it (Arnold [15]).

Depending on presence of particular components of the stress tensor, types of pressures are defined. (Kamarád [14])

Hydrostatic pressure (a liquid or a gas transmitting medium)	$\sigma_{11} = \sigma_{22} = \sigma_{33}$ $P = -\sigma_{11} = -\sigma_{22} = -\sigma_{33};\ \sigma_{ij} = 0, i \neq j$
Quasi-hydrostatic pressure (a solid transmitting medium)	$\sigma_{11} \neq \sigma_{22} \neq \sigma_{33}$ $P = -1/3 \sum \sigma_{ii};\quad \sigma_{ij} \neq 0, i \neq j$
Uniaxial pressure (without a transmitting medium)	$\sigma_{11} \neq 0, \sigma_{22} = \sigma_{33} = 0$ $P = -\sigma_{11}/3$ shear stress σ_s in a general plane under an α-angle to x_1-axes: $\sigma_s = \sigma_{11} \cos\alpha \sin\alpha$

2.3.2 Pressure influence

The pressure application results in changes of linear dimensions and volume of the crystal lattice and thus in energy changes of a given system. The compressibility and its anisotropy should be closely considered when considering the impact of pressure on a crystal lattice. The resulting effects are for example variation of exchange interaction, delocalisation of the electrons, changes of the atoms-binding character, energy-gap variation, hybridisation or core ionisation, leading for example to formation of metallic state in inert gases, changes in electrical conductivity or structural transitions (Arnold [15]; Sikka and Vijayakumar [16]).

Localized magnetic moment-systems

The rare-earth-element ions have localized magnetic moments (origination in the 4*f*-electrons) at ambient pressure that are very stable up to very high pressures that are able to change the electron occupation of non-filled inner atomic shells or change the 4*f*-electron character from localized to itinerant (Kamarád [17]; Sikka and Vijayakumar [16]). The pressure influence on the value of the transition temperatures T_C or T_N is mainly connected with

the pressure effect on the exchange interaction integral J, where $|J| = 3kT_{C,N} / 2zS(S+1)$, k is the Boltzmann constant and z is the coordination number, due to relation:

$$d\ln J / d\ln V = d\ln T_{C,N} / d\ln V \equiv \Gamma, \tag{2.24}$$

where Γ is so called Grüneisen parameter.

Itinerant electrons-systems

The parameters appearing in the itinerant-electrons model of magnetism, the electron-electron interaction U and the density of states at the Fermi level $N(E_F)$, are very sensitive to a variation of interatomic distances. In general, application of a pressure leads to an increase in the interaction and to decrease in the $N(E_F)$, the particular dependencies being influenced by many factors as e.g. the crystal lattice symmetry, coordination number or the short-range order of atoms (Kamarád [17]).

For the transition-metal ferromagnets, Wohlfarth et al. [17] derived two limiting cases of the transition-temperature dependence on pressure. In the strong itinerant ferromagnets, T_C should increases with pressure as

$$dT_C / dp \sim \lambda \kappa T_C \quad \text{and} \quad \Gamma \sim -\lambda, \quad -\lambda \equiv d\ln W / d\ln V, \tag{2.25}$$

where W is the width of the electron energy band. In the very weak itinerant ferromagnets, T_C decreases with pressure according to relation

$$dT_C / dp \sim -A_W / T_C \quad \text{and} \quad \Gamma \sim \lambda S, \tag{2.26}$$

where A_W is the Wohlfarth constant and S is the Stoner factor.

For systems with fluctuations, the Curie temperature depends linearly on the applied pressure as (Mohn et al. [4, 10])

$$T_C(P) = T_{C,0}\left(1 - \frac{P}{P_C}\right), \tag{2.27}$$

where P_c is the critical pressure for the disappearance of magnetism.

Chapter 3 Previous results on studied materials in literature and motivations of this thesis

3.1 Cubic Laves phase structure

All the compounds measured in this work ($ErAl_2$, $ErCo_2$ and $Er(Co_{0.975}Si_{0.025})_2$) crystallize in cubic Laves phase ($MgCu_2$-type structure, belonging to the space group Fd-3m – e.g. Konopka et al. [18]; Iandelli and Palenzona [19]; Cuong et al. [20-22]) in which the rare-earth ions lie on a diamond lattice.
As for the $ErCo_2$ compound, the unit cell of this structure contains 8 formula units. The compound consists of two sublattices whereas the R atoms lie at position (8a) (0, 0, 0) and the remaining space inside the cell at the position (16d) (0.625, 0.625, 0.625) is occupied by regular tetrahedral consisting of the Co atoms.

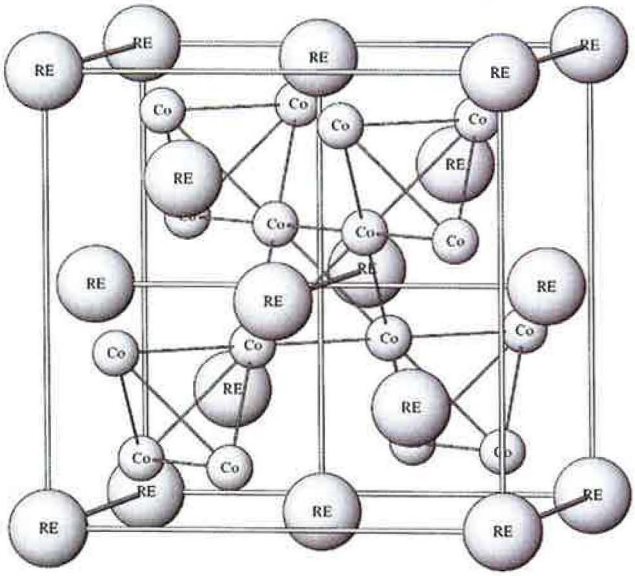

Figure 3.1

3.2 $ErAl_2$ compound

The $ErAl_2$ compound orders ferromagnetically at Curie temperature $T_C \sim 10$-14 K (e.g. Inoue et al. [23]; Levin et al. [24]; Boucherle et al. [25]). The ordered state is characterized by the easy magnetization axis [111] (Purwins et al. [26, 27]; Levin et al. [24]) and it exists due to the indirect spin exchange interaction between the localized magnetic moments on rare-earth atoms via conduction electrons – RKKY (Campoy et al. [28]). Purwins et al. [26] obtained saturated magnetic $7.6\mu_B$ indicating a sizeable quenching of the free-ion moment. The main interest in the past was laid in the studies of the cubic crystalline electric field that is experienced by the 4f electrons.

3.3 $RECo_2$ (RE = rear earth atom) compounds

3.3.1 $RECo_2$ compounds and itinerant electron metamagnetism

Introduction

Within the series of RET_2 (RE = rare-earth atoms and Y; T = Fe, Co, Ni) intermetallics, the $RECo_2$ family has attracted most attention because of magnetic instabilities in the Co sublattice. If we look on the compounds with iron and nickel the situation is not as complex. In the $REFe_2$ compounds, the Fe sublattice satisfies the Stoner criterion (Giorgetti et al. [29]) so the Fe-moments are more or less independent, no matter if the RE-ions bear a magnetic moment or not. In $RENi_2$ compounds, the Ni sublattice (owing to the position of the Fermi level lying in the flat low density-of-3*d*-states region) bears no magnetic moment even in compounds with magnetic RE-ions (Garcia et al. [30, 31]). But in $RECo_2$, the magnetic moment of the cobalt sublattice depends strongly on the existence of a moment on the RE-sites, on its type and the concentration of the RE-ions (Baranov et al. [32]). Because the Co 3*d*-band states appear near the critical conditions for magnetic-moment formation, the $RECo_2$ compounds offer an opportunity to study various aspects of the itinerant electron metamagnetism. The Co magnetic moment may be formed and ferromagnetically ordered in a magnetic field which is sufficiently high to induce a metamagnetic transition (MT) connected with a sudden splitting of the Co majority and minority 3*d* subbands.

The $RECo_2$ compounds with nonmagnetic rare earth element (RE = Y, Lu) are the strongly exchange-enhanced Pauli paramagnets that undergo a metamagnetic transition at low temperatures by applying a critical external magnetic field larger than ~ 70 T (Goto et al. [33, 34]).
On the other hand, when the RE elements are magnetic (RE = Dy-Er) the Co metamagnetic state may be achieved in zero external field due to the large internal exchange field created by the ferromagnetically ordered 4*f* magnetic moments at the transition temperature T_C. In other $RECo_2$ compounds with other magnetic RE elements (except for Ce and Tm), the Co bears a stable magnetic moment. When the compounds contain light magnetic RE atoms they are ferromagnets (the RE and Co moments are parallel) while the ones with heavy magnetic RE atoms are ferromagnets (the Co moments are antiparallel to the RE ones).
In the compounds $ErCo_2$, $HoCo_2$ and $DyCo_2$, the first-order magnetic phase transition is observed at T_C. The changes in the 3*d*-band structure within the series controlled by the variation of the lattice parameter (due to the lanthanide contraction) have been found to be the reason for the first-order transition (Khmelevskyi et al. [35]) that should change into the second-order one by diluting the magnetic RE atoms (for example by nonmagnetic Y atoms (ref. in Hauser et al. [36])) or by applying the pressure (Bloch and Edwards [37]; Inoue and Shimizu [38, 39]). In conjunction with electronic structure, the first order transition should be closely connected with the existence of metamagnetic behaviour of the Co subsystem (Gratz and Markosyan [40]) and numerous experiments are focused on understanding this feature. Further, the $ErCo_2$ compound is particularly interesting because the internal exchange field created by Er moments is just above the critical value for inducing MT in the Co sublattice.

Itinerant electron metamagnetism

The itinerant electron metamagnetism (IEM) is a field-induced first-order magnetic transition in an itinerant electron system at a critical field, predicted first by Wohlfarth and

Rhodes [41] for compounds having a highly enhanced Stoner factor and exhibiting a strong energy dependency of the density of states (DOS) along with a positive curvature in the vicinity of the Fermi level. The transition can be from a paramagnetic into a ferromagnetic state or, in the case of ferromagnetic ground state, from a weak ferromagnetic to a strong ferromagnetic state (Gratz and Markosyan [40]).

3.3.2 Composition of $RECo_2$

It has been reported in many experimental works that for the preparation of a single-phase $RECo_2$ sample an excess of the RE component is necessary. The starting composition proposed by different authors varies between 1:1.88 and 1:1.95. This off-stoichiometry is explained by avoiding the origination of $RECo_3$ phase (for example Syshchenko et al. [42]). Gratz and Markosyan [40] take notice that the weight loss observed during the melting procedure being within 0.1% (i.e. it is much less to shift the composition to 1:2) so they do not accept the idea of a preferential evaporation of the RE component but they propose the off-stoichiometry should be caused by RE-atoms partly occupying the transition metal sites in the tetrahedral. Anyway, it is necessary to avoid the origination of the $RECo_3$ phase because it is ferromagnetic already at room temperature (Syshchenko et al. [42]) and this can be harmful to absolute values of magnetic susceptibility data of paramagnetic $RECo_2$.-matrix even if present as a spurious phase of the concentration of fractions of percent.

3.3.3 Electronic and magnetic properties of the $RECo_2$ compounds with special interest in $ErCo_2$

In the $RECo_2$ (RE=magnetic rear-earth atoms), the 4*f*-electron states of the rare-earth atoms are well localized which prevents an overlapping between these states and the other atoms of the material. The important interaction between the RE and Co atoms is provided via the wide 5*d*-band states of the RE-ions. Because of the positive 4*f*-5*d* intra-atomic coupling (4*f*-electron spin moments are parallel oriented to the 5*d* ones) the 5*d*-states become polarized and consequently the association of them together with narrow 3*d*-bands with lower energy forms the $RECo_2$ compounds. The electronegativity difference between the Fermi energies of the pure metals gives rise to a transfer of the 5*d*-electrons to the unfilled 3*d*-band. Because the screening of nuclear potentials by the electrons is modified, the two *d*-bands draw together. The resulting hybridisation of the 3*d* and 5*d* states leads to a ferromagnetic coupling between their spins (Gignoux et al. [7]) and consequently, due to the Hund's rules, the total magnetic moment M_R is oriented antiparallel to the transition metal moment M_T for heavy and parallel to the M_T for light rare-earth atoms (Gratz and Markosyan [40]).

Also, there is created a region of a positive curvature in the DOS From band-structure calculations (Garcia et al. and ref. therein [30]), it has been concluded that most of the properties observed in the $RECo_2$ compounds could be understood by considering the Fermi-level position E_F that is situated near a local peak of the curve of the DOS. The high value together with a special shape of the DOS-curves in the vicinity of the E_F give rise to spin fluctuations in the 3*d*-band that are also responsible for the occurrence of IEM.

In the paramagnetic state, there are spin-disorder scattering on paramagnetic rare-earth moments and electron spin-fluctuation scattering depending on the dynamics of spin fluctuations in the Co 3d-band (Duc et al. [43]). When the temperature is decreased the 4*f*-moments order ferromagnetically at Currie temperature T_C and via the 5*d*-3*d* hybridisation

they cause a large effective exchange field acting on the Co 3*d* states (Syshchenko et al. [42, 44, 45]). If this is sufficient to split the 3*d* majority and minority subbands, the spin fluctuations at the Co-sites are quenched and the 3*d*-band metamagnetic state is induced by the first order transition. This occurs as an abrupt jump in specific heat, magnetization, susceptibility or electrical resistivity (Imai et al. [46]; Vasylyev et al. [47]; Wada et al. [48]; Soares et al. [49]; Cuong et al. [20, 50, 51]; Danis et al. [52]; Duc et al.[43, 53-55]; Woo et al. [56]; Garcia et al.[30, 31, 57]; Prokleska et al. [58]), magnetovolume effect and the crystal lattice undergoes a rhombohedral distortion (Danis et al. [52]).

The electronic structure was approved even by microscopic-methods (neutron diffraction and XMCD measurement (Moon,et al. [59]; Herrero et al.[60-62]); Giorgetti et al. [29]) and the ferrimagnetic coupling of Er and Co with magnetic moments μ_{Er} = (8.84 ± 0.06) μ_B and μ_{Co} = (0.95 ± 0.03) μ_B (at 5K) was confirmed (Herrero et al. [62]). In the ordered state, the Er- and Co-magnetic moments are aligned along the [111] direction (Atzmony et al. [63]).

3.3.4 Theoretical background

Introduction

For appearance of Co-magnetic moments and their ferromagnetic ordering in a $RECo_2$ system, effective magnetic field must reach the value of the magnetic field necessary for inducing the metamagnetic transition of the Co sublattice B_0. The effective field can be described as (Gratz and Markosyan [40]; Bartashevich et al. [64])

$$\vec{B}_{eff}^{Co} = \vec{B}_{mol}^{Co} + \vec{B}_{ext} = \vec{B}_{RCo}^{Co} + \vec{B}_{CoCo} + \vec{B}_{ext} = n_{RCo}\vec{M}_R + n_{CoCo}\vec{M}_{Co} + \vec{B}_{ext.} \qquad (3.1)$$

where $\vec{B}_{RCo}^{Co}$ and $\vec{B}_{CoCo}$ are the fields arisen from the intersublattice and intrasublattice exchange interactions, respectively, and n_{RCo} and n_{CoCo} are the corresponding molecular field coefficients. As for the field B_{RCo}^{Co} , it is

$$B_{RCo}^{Co} \propto I\,(g_J - 1)\,J_R\,, \qquad (3.2)$$

where g_J is the Lande factor associated with the total magnetic momentum J_R and I is the exchange coupling constant (Hauser et al. [36]). Also it especially holds that

$$B_{eff}^{Co} = B_{ext} - B_{mol}^{Co}\ . \qquad (3.3)$$

This follows from the fact that in all $RECo_2$ compounds the M_R is larger than the M_{Co} and an applied field is then parallel to the M_R. Also, the molecular field points in the antiparallel direction to the M_R and so the effective field decreases (for heavy $RECo_2$) with an increasing applied field. The Co magnetization can be destabilized if the applied field exceeds a critical field B_{cr}. After, so called inverse IEM occurs and under higher fields only a long-range magnetic order exists in the R sublattice (Bartashevich et al. [64]).

The field B_0 was found experimentally to be $B_0 \sim 70$ T (Goto et al.[33, 34]). As for the $ErCo_2$ compound, the value of molecular field is B_{mol}^{Co} = 190 T, the lowest among the heavy $RECo_2$ compounds (Gratz and Markosyan [40]), the critical field is 52 T (Bartashevich et al. [64]).

As mentioned before, almost all the $RECo_2$ order by the second-order transition (SOT) type, just with the exception of $DyCo_2$, $HoCo_2$ and $ErCo_2$. During the years, lot of phenomenological models have been proposed because of describing properly the condition for the first-order transition (FOT) type appearance.
Considering the Landau expansion of the magnetic free energy F referred to the $3d$-electron-subsystem magnetization, Bloch et al. [37] connected the FOT occurrence at T_C with the negative sign of the Landau coefficient $B(T)$

$$F(M_d) = \tfrac{1}{2} A(T) M_d^{\,2} + \tfrac{1}{4} B(T) M_d^{\,4} + \tfrac{1}{6} C(T) M_d^{\,6} \qquad (3.4)$$

and with the critical temperature for the $B(T)$ sign change about 200K. Later, this model was improved and extended for the IEM theory by Inoue and Shimizu [38] by expanding the free energy in terms of the total magnetization of a system M.
Contrary, Khmelevskyi and Mohn [35] relate the transition type to lattice parameter and certain characteristics of the electronic structure.

Substitutions and pressure influences

As mentioned above, the condition for Co-magnetism appearance is dependent on substitutions or a pressure application; the internal field B_{RCo}^{Co} or the critical field B_0 are influenced (e.g. Hauser et al. [36]; Yamada [65-67]). After, this should be proved by a transition temperature shift and even by the change in type of the transition order or the Co-magnetism suppression (e.g. Bartashevich et al. [64]; Cuong et al. [20, 50, 51]; Garcia et al. [30, 31]; Ishimatsu et al. [68]; Liu and Altounian [69]; de Oliveira et al. [70]; Prokleška et al. [58]; Soares et al. [49]; Syshchenko et al. [42, 44, 45]; Vasylyev et al. [47]).

Hauser et al. observed for the first time separated ordering of the R- and the Co-sublattice for some limited concentration range ($x_1 < x < x_2$) in the $Er_{1-x}Y_xCo_2$ system. At the temperature that the R sublattice orders, $B_{RCo}^{Co} < B_0$, and so $T = T_C^R$. First with further cooling, the conditions for the Co-sublattice are fulfilled and it orders (by the first order transition as follows from the metamagnetic character of the process) at $T = T_C^{Co} < T_C^R$. With further Y-content increase, only R-sublattice proves long-range magnetic order and finally even this disappears.
They predict similar effect caused by the pressure application. Based on the Yamada's calculation showing that $H_{cr}(P)$ has to increase with increasing pressure and assuming negligible influence of the B_{RCo}^{Co} by pressure, they anticipate the existence of the critical pressure P_{cr}, at wich the transition-order type is changed, and a limited pressure range with separate transition-temperature appearance.

3.3.5 Parrimagnetism

The processes that come about in the paramagnetic state seem to be rather clear, as presented further. But recently presented results from Herrero et al. [60-62] has opened question what exactly happens at the transition temperature T_C. They reminded that already earlier another authors concluded from their experiments in existence of Co-magnetic moment in the paramagnetic phase (e.g. Liu and Altounian [71]).

Herrero et al. investigated in detail the $ErCo_2$ paramagnetic phase by means of XMCD[2], small-angle neutron scattering and AC magnetic susceptibility measurements as a function of temperature and magnetic field. Analyzing the resulting data, they discovered that the Co bears a net magnetic moment well above the ferrimagnetic transition temperature (Fig. 3.2a) that is connected with the occurrence of a short-range magnetic order originating in formation of ferromagnetically coupled Co-magnetic clusters. They denoted this phenomenon as parimagnetism. They expect similar behaviour also in the other ferrimagnetic $RECo_2$ compounds, moreover they suggest that the parimagnetism could be a general feature of ferrimagnetic materials.

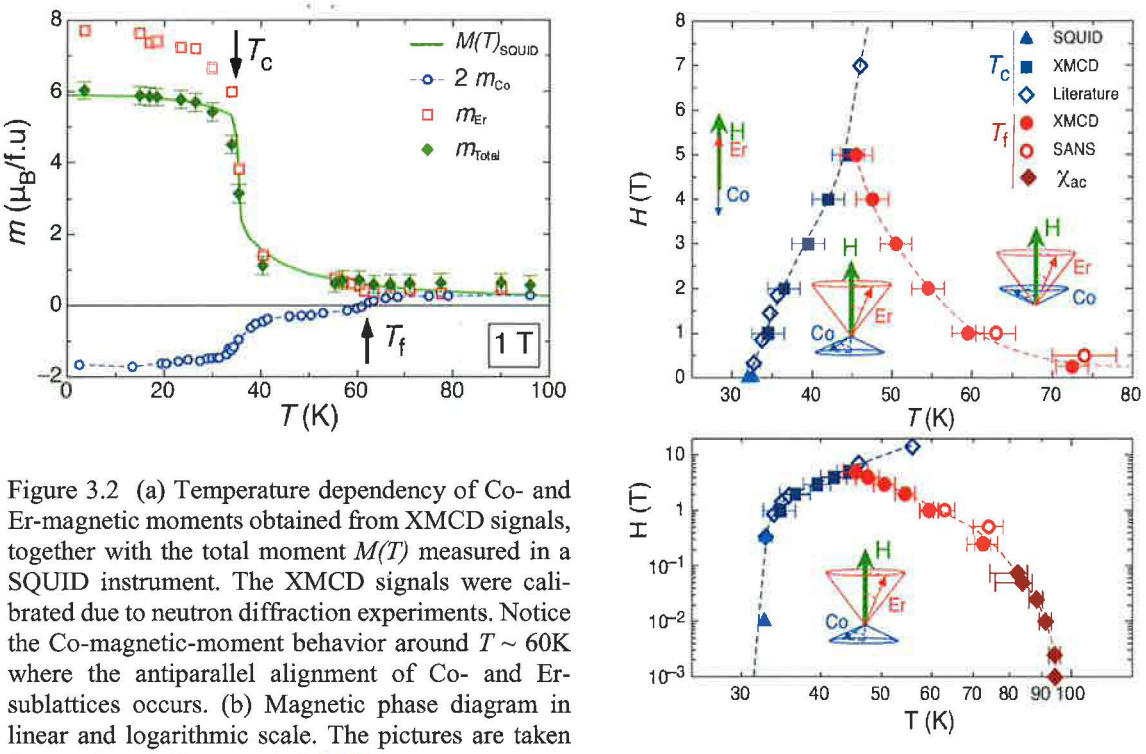

Figure 3.2 (a) Temperature dependency of Co- and Er-magnetic moments obtained from XMCD signals, together with the total moment *M(T)* measured in a SQUID instrument. The XMCD signals were calibrated due to neutron diffraction experiments. Notice the Co-magnetic-moment behavior around $T \sim 60K$ where the antiparallel alignment of Co- and Er-sublattices occurs. (b) Magnetic phase diagram in linear and logarithmic scale. The pictures are taken from reference Herrero et al. [62].

They explain the origination of the resulting state observable in the system as a consequence of the competition of an applied and exchange field acting on the Co moments (Fig. 3.2b). At low temperatures (under T_C), the Co-magnetic sublattice is ordered antiparallel to the Er one owing to the dominating Co-Er exchange interactions. At the T_C, the Co magnetization proves an abrupt jump so that (under low applied magnetic fields – up to 5T) the net magnetization decreases significantly but the two sublattices are still antiparallel aligned. With further increase of the temperature, the Co magnetization shows an another abrupt jump, goes through the zero value and changes its sign (flips) at the flipping temperature T_F. Above the T_F, the applied field dominates to the whole system and so the Co- (and Er) net magnetization is parallel to it.

For flipping the orientation of a single Co moment, the Co-Co exchange interactions[3] are to be overcame. It is energetically favourable if the process takes place in a collective way in clusters so that the number of antiparallel Co-Co neighbours is minimized. Such clusters are

[2] Measurements were performed at the Co $L_{2,3}$ and Er $M_{4,5}$ absorption edges – this allows to explore the Co 3d and Er 4f empty states (Herrero et al. [62]).

[3] The Co-Co interactions are the strongest interactions in the system.

estimated to have size 7-8 Å and include from 30 to 50 Er atoms and 60 to 100 Co atoms bearing exclusively low-spin moment.

Chapter 4 Experimental methods applied

4.1 Sample preparation

The single crystal $ErAl_2$ sample was prepared by Hidenori Miyagawa, a PhD. Student at Kyushu University in Japan.

The polycrystalline $ErCo_2$ and $Er(Si_{0.025}Co_{0..975})_2$ samples were prepared by arc melting in mono-arc furnace in the Technology Laboratory of the Department of Condensed Matter Physics (DCMP), Faculty of Mathematics and Physics, Charles University in Prague. For the syntheses, constituent elements of the following purities were used: Er of 4N, Co of 4N and Si of 5N. For further improving of the purity, Er-material was either refined by solid-state electro-transport ($ErCo_2$) or three times pre-melted ($ErCo_{1.975}Si_{0.025}$) in mono-arc furnace.
For preventing formation of the $ErCo_3$ spurious phase, erbium was added over the stoichiometric amount in the final ratio Er:Co, respectively Er:(Co,Si), as 1:1.95. In order to achieve a good homogeneity, the samples were twice remelted and after it the resulting polycrystalline ingots were wrapped up in a tantalum foil, sealed in quartz tubes and annealed under Ar atmosphere at 850°C for a weak.

The mono-arc apparatus consists of a sample's chamber, a tungsten torch, vacuum system, water-cooling system and power supply for the arc. The constituent elements are set in the water-cooled copper crucible inside the chamber, evacuated to a pressure $\sim 1.33.10^{-2}$Pa and then filled by protective argon atmosphere. As the crucible is continuously cooled during melting, the surface tension of the melt holds the drop of the material without a thermal contact with the material of the crucible and avoids any contamination of the melt (Vejpravová [72]).

4.2 Sample characterization

4.2.1 X-ray powder diffraction

The prepared samples were analysed by the powder X-ray diffraction (XRD) at room temperature by means of Seifert XRD7 and Bruker diffractometer at DCMP working with the Bragg-Bretano geometry. XRD patterns were recorded using the Cu K_α radiation (λ = 1.54Å). The 2Θ scans were performed within 10 - 130 range by a 0.02-step with a 5 seconds exposition per point. Obtained data were analysed by the Fullprof program [73] using the Rietveld analysis that refines crystallographic parameters and eventually determines impurities if the crystallographic model of the studied sample is known.

4.2.2 Microprobe analysis

For proving the quality of prepared sample - their homogeneity and stoichiometry, investigation with the field-emission high resolution scanning electron microscope (SEM) giving a

over-viewing information about the sample-surface composition and with energy dispersive X-ray analysis (EDAX) detector identifying in detail the element composition of a chosen point.

4.3 Bulk investigation techniques

4.3.1 Magnetization measurements

Measurements of AC magnetic susceptibility and DC magnetization were performed in Magnetic Property Measurement System - Superconducting Quantum Interference Device (SQUID) magnetometer [74] and Physical Properties Measurement System (PPMS) instrument [75] (both from Quantum Design), installed in the Joint Laboratory for Magnetic Studies of the Charles University, Faculty of Mathematics and Physics and the Institute of Physics ASCR, v.v.i. in the Faculty Campus in Troja.
Magnetization measurements at ambient pressure were performed either on bars (for a single crystal sample) or on powders (for polycrystalline samples). The measurements at an applied pressure were performed on bars. In the case of powders, a fixed-powder or a free-powder method were used. The first one imitates the experiment on an ideal poly- crystalline sample proving qualitative properties of a magnetic system, the further one allows considering a sample as the assembly of small single crystals orienting freely in the direction of an applied magnetic field proving quantitative properties of a system.
Typically, AC-susceptibility data at ambient pressure were collected at the frequencies from 10Hz to 10kHz with the drive amplitude of the AC magnetic field 0.2 mT. For measurements under applied pressure, one had to take into account the sensitivity of the used pressure cell to a used frequency[4] and so f =1 and 213 Hz (see further) were used.

PPMS instrument

As for DC measurements, a constant field is applied to the measurement region and a sample is moved quickly through detection coils, inducing a signal in them according to the Faraday's law. Magnetic moment in order 10^{-2} Am can be detected like this.
During AC measurements, an alternating field is applied to the measurement region and a sample is positioned in the center of each detection coil. The detection coils indicate, how the applied field is altered by the presence of the sample. This method does not directly measure a sample's magnetic moment, but it is very useful for examining the nature of magnetic phase transitions. This method allows detecting magnetic moments in order 10^{-5} Am.

SQUID magnetometer

The SQUID magnetometer [76, 77] is the modification of an extraction magnetometer where the variation of magnetic flux due to the movement of a sample is transformed into voltage in pick up coils. But in order to increase the sensitivity, there are superconducting-coil rings containing two parallel Josephson's junctions. If constant biasing current is maintained in the device, the measured voltage oscillates with the changes in phase at the two junctions, which depends upon the change in the magnetic flux. Counting the oscillations allows evaluating the flux change that has occurred. As a result, it is possible to register magnetic

[4] The applied field causes vortex currents dependent on the frequency.

moments as small as 10^{-11} Am^2. The magnetometer provides a controlled environment with available temperature range from 5K to 300K and fields 0T - 5T.

Demagnetising factor

The experimental results of magnetic measurements are mostly affected with the so-called demagnetising factor [2], which represents interaction of the "sample geometry" with an external magnetic field. When inserting a sample in the magnetic field the intensity of a magnetic field around and in the sample will change. The relation between the external H_e and the internal magnetic field H_i is given as

$$\vec{H}_i = \vec{H}_e - \vec{H}_d , \tag{4.2}$$

where H_d is the demagnetising field proportional to sample's magnetization M as

$$\vec{H}_d = D\vec{M} , \tag{4.3}$$

where D is the demagnetising factor – the tensor for a general-shaped sample. For realizing the internal magnetic field from measured data, the method described in Brož [78] was used.

4.3.2 Electric resistivity measurements

The measurements of electric resistivity were performed on bar-shaped samples in the PPMS [75] and in Closed Cycle Refrigerator instrument [79]. Standard technique for electrical-transport measurements, the four-probe AC method, was used both in ambient- and applied-pressure-experiments. The benefit of this method consists in eliminating the contribution of contacts in a measured signal (Brož [78]).
The applied AC current was typically of the amplitude 10 mA and frequency 37 Hz. For measurements at ambient pressure, samples were placed in the special puck for electric-transport measurement from Quantum Design (see the Figure 4.1), connected with copper wires of 100 or 50 μm diameter and attached with a silver paint. Measurements under pressures are described in the next chapter.
The main contribution to the error of measurements comes from determining the sample cross-section and the distance between the voltage contacts.

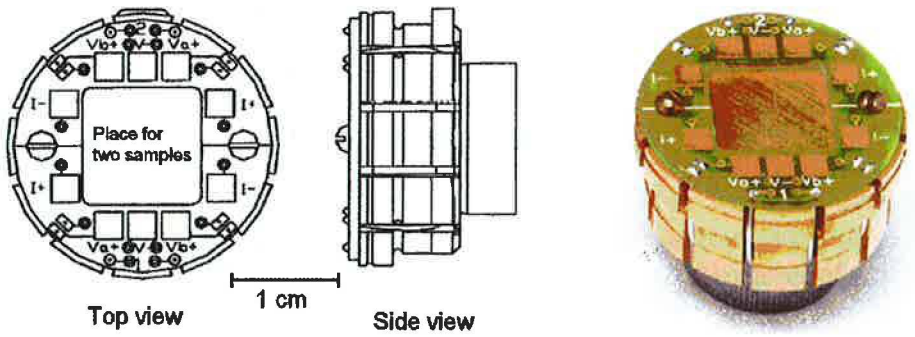

Figure 4.1 Puck for electric-transport measurement at ambient pressure from Quantum Design.

4.4 Pressure techniques

Depending on the type of desired experiment, hydrostatic clamp pressure cells (CPC) with a liquid pressure-transmitting medium, uniaxial-pressure cell or Bridgman-type cell with a solid pressure-transmitting medium were used in our measurements.
Especially for the hydrostatic CPC holds that because of different thermal expansion of the pressure transmitting medium and the construction materials of the cells, the pressure changes during cooling or heating (see Appendix A) for the experimentally realized differences among typically used liquid transmitting media [80].

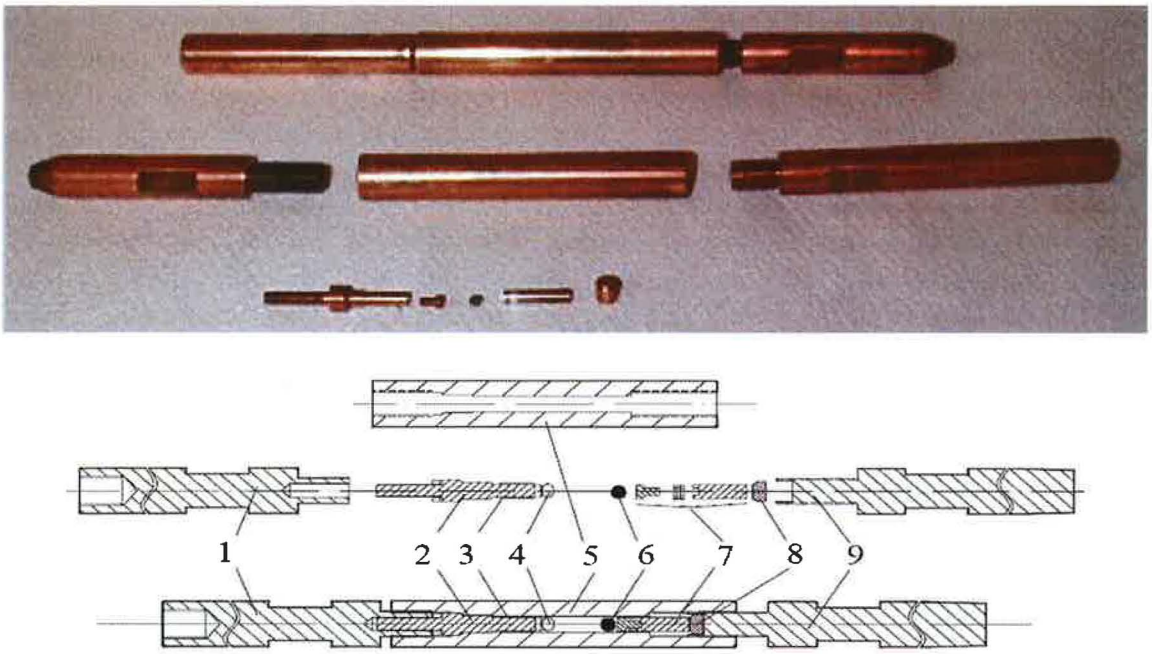

Figure 4.2 Hydrostatic clamp pressure cell for ACMS measurements in SQUID magnetometer. Inner diameter is 2.5mm and outer diameter is 8.6mm. Upper and lower pressure clamping bolts (1,9), plug (2) with sealing (3), sample on a holder (4), pressure cell (5), lead pressure manometr (6), piston with Bridgman mushroom-type seal (7), piston backup (8). Taken from Ref. [80].

4.4.1 Hydrostatic clamp pressure cells

Magnetization measurement

For magnetisation and AC-susceptibility measurements, the pressure cell designed by Dr. J. Kamarád[5] especially for usage in SQUID magnetometer was used (Figure 4.2). The cell-dimension and used material from annealed copper-beryllium-bronze (CuBe) confine the measurements under pressures up to ~1.2 GPa. A standard Bridgman-type of seal is used on a piston (Arnold [15]).; the plug with a sample's holder is sealed by a set of Cu- and plastic-rings. As a pressure-transmitting medium, the spindle oil (OL3) was used.
Pressure is determined at low-temperature region from the well-known pressure dependence of the critical temperature $T_c(P)$ of the superconducting transition of lead. The super-

[5] High Pressure Laboratory, Academy of Science, Prague, Czech Republic.

conducting temperature T_c decreases with applied pressure and the pressure is given as

$$P[kb] = \{T_c(0) - T_c(P)\}/0.0405, \tag{4.4}$$

where the values of T_c at ambient and high pressures are derived from temperature dependence of AC-susceptibility of lead in the SQUID magnetometer (Arnold [15]).

Resistivity measurement

For direct electric-resistivity measurements, the hydrostatic double-layer CPC (composed from CuBe and NiCrAl alloy) designed by Dr. Naka[6] was used (see Fig. 4.3). The cell is originally determined for the PPMS instrument but thanks to appropriate modifications experiments were performed also in the Closed Cycle Refrigerator instrument.
This cell is constructed for measurements under pressures up to 3GPa. Sample and manganin manometer are hidden in a teflon container (2.7mm) filled with a pressure transmitting medium (Daphne oil 7373) inside of the inner space of the pressure cell with diameter 4mm. The resistivity of the sample is measured with the standard four-point method (see Fig. 4.4a). The copper wires (50 μm) are attached to samples with silver epoxid[7] and lead out of the pressure cell through the plug and are fixed on the standard electric Quantum-Design-connector attached to this plug that allows usage in both the PPMS or Closed Cycle Refrigerator.
Pressure inside this cell is determined by the linear pressure dependence of the electrical resistivity of a manganin. The used manganin manometer is prepared as a coil - wound bifilarly using the manganin wire, twice spun round with silk. The electrical resistivity at room temperature and at ambient pressure of the final coil is about 40-80 Ω, the respective resistance-pressure dependence is given as

$$R(T,P) = R(T,0)\left[1 + P \cdot \alpha(T)\right] ,$$

$$P = \frac{R(T,P) - R(T,0)}{R(T,0)} \frac{1}{\alpha} , \tag{4.5}$$

where $R(T,P)$ and $R(T,0)$ are the values of the electrical resistance of the manganin at temperature T and at pressure P or at ambient pressure; $\alpha(T)$ is a pressure coefficient of the manganin's resistance that depends on the diameter of the manganin ($\alpha(293K)$ = 0.00246 GPa^{-1} in our experiments).

AC-susceptibility measurement

For AC-measurements under higher pressures, the (previously described) clamped pressure cell was especially modified by Mgr. M. Míšek[8] so that a miniature coil made of copper wire was put directly around the sample. In the time of the running experiments the coil was not calibrated so only relative values could have been taken.

---

[6] National Institute for Materials Science, Tsukuba, Japan.

[7] Attachment with silver paint was found as insufficient.

[8] Department of Condensed Matter Physics, Charles University in Prague, Czech Republic.

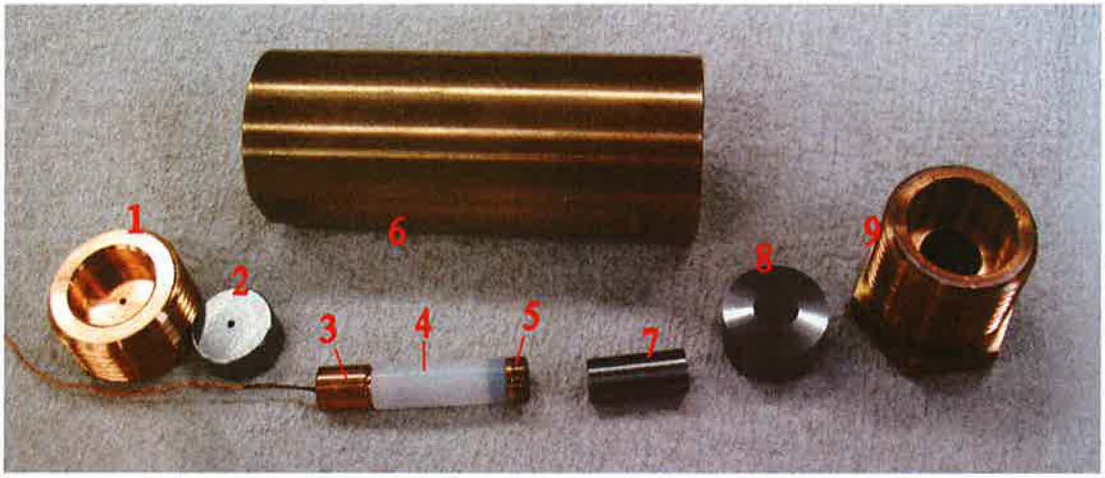

Figure 4.3 Hydrostatic clamped pressure cell for electric resistivity and AC susceptibility measurements in PPMS and CCR instruments. Inner diameter is 4mm, working-space diameter is 2.7mm. Upper and lower pressure clamping bolts (1,9); plug (3) with a protective teflon container (4) covering a sample and the manganin pressure manometer ; Cu sealing (5); pressure cell (6); piston (7).

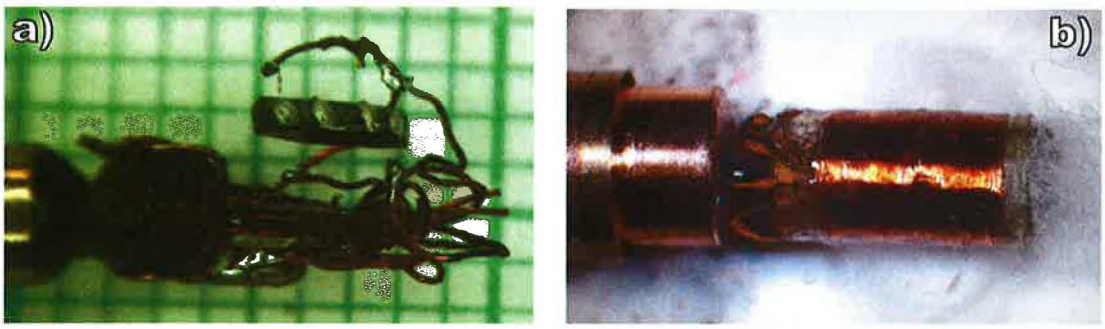

Figure 4.4 Detailed view on experiment's arrangement for the hydrostatic clamped pressure cell. Sample's space after electric resistivity measurement (a) – noticeable contacting of the sample and the manganin-manometer. Demonstration installation of the miniature coil for a AC-susceptibility measurement (b).

4.4.3 Diamond anvil cells

For measurements of electric resistivity under very high pressures (above 3GPa), the Bridgman type of cell designed by Dr. Griveau[9] was used. See Fig. 4.5 and 4.6.
The design is based on the original principles of diamond anvil cell (Eremets [81]). A sample is placed in between precisely parallel faces of two anvils that are in our case made from tungsten-carbide (TC). The working space is confined by a steatite ($MgSiO_3$) gasket ring that has in our case an inner diameter of 1 mm. The parameters allow placing of a sample of thickness up to 60 μm. The resistivity is measured with help of platinum wires of 20μm.A pyrophyllite ($AlSi_2O_5OH$) disc is used as the pressure-transmitting medium. Pressure inside the cell is determined by the superconducting transition of lead (see higher). The maximum pressure allowed in this cell is 20 GPa (with safe pressure up to 12-13 GPa).

[9] Joint Research Centre, Institute for Transuran Elements, Karlsruhe, Germany.

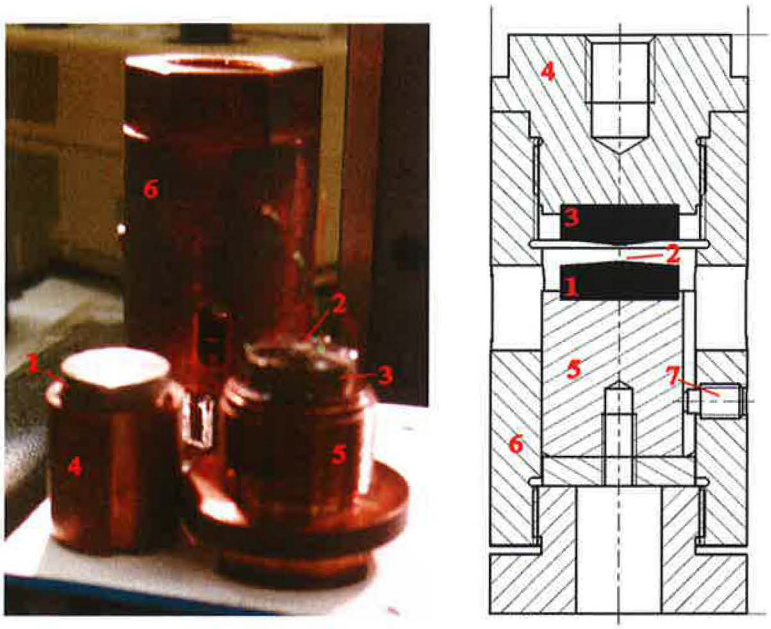

Figure 4.5 Bridgman type of cell for electric resistivity measurement. 1,3 – upper and lower anvils (WC), 2 – working space of 1mm arisen from a steatite-gasket confinement, 4,5 – anvil support (CuBe), 6 –pressure cell body (CuBe), 7 – adjusting screw

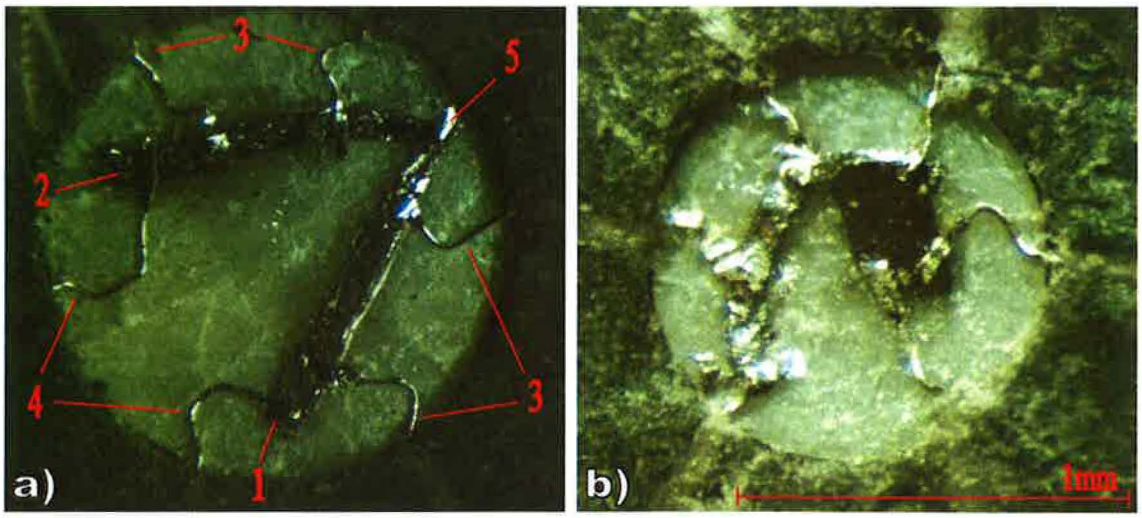

Figure 4.6 Detailed view on experiment's arrangement in a Bridgman-type of cell. Ideal installation (a) (not prepared for our measurements); sample (1) and lead pressure manometer (2), pairs of voltage contacts for sample and manometer (3), shared current contacts (4) -- used owing to the fact that sample and manometer are in a touch (5). Installation for experiment on $ErCo_2$ sample.

4.4.2 Uniaxial pressure cell

For uniaxial-pressure experiments of magnetisation and AC susceptibility, the miniature uniaxial pressure cell designed by Dr. J. Kamarád[10] for the SQUID magnetometer was used (Fig. 4.7).

[10] High Pressure Laboratory, Academy of Science, Prague, Czech Republic.

Before a usage, the force developed on a system is calibrated for appropriate screw-displacement. Oriented single crystal is placed between ZrO-ceramic pistons and smoothly squeezed-up to a sample yield stress by a force of up to 20 kN produced by Belleville springs (Kamarád et al. [82]).

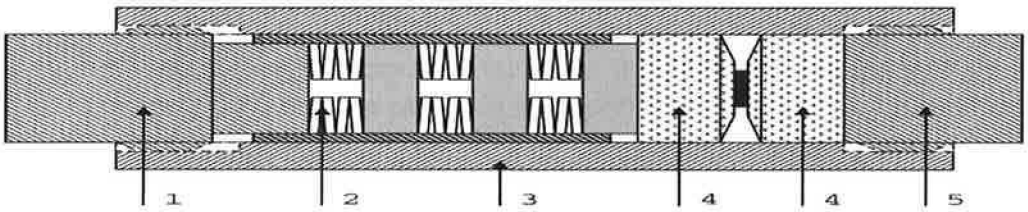

Figure 4.7 Uniaxial pressure cell for ACMS measurements in SQUID magnetometer. Squeezing screw from CuBe (1), set of Belleville springs (2), pressure cell from CuBe (3), ZrO-ceramic pistons (4), fixing screw from CuBe (5)

Chapter 5 Properties of $ErAl_2$ compound

5.1 Results and discussion

On a single crystal of $ErAl_2$ compound, magnetic measurements (magnetization and AC susceptibility) along the magnetic easy axis were performed at ambient pressure and under applied hydrostatic and uniaxial pressure in appropriate pressure cells.

5.1.1 Magnetic properties at ambient pressure

The field dependent magnetization *M(H)* measurements were performed at 2 K and around the transition temperature, from 5 K to 15 K with a 0.8 K-step. Selected curves are presented in Fig. 5.1a. The temperature dependent AC susceptibility measurement $\chi(T)$ were done under zero applied DC magnetic field. The transition temperature was determined as T_C = 11K from the position of the $\chi(T)$ peak (Fig. 5.1b). Nearly the same value can be determined from the Arrott –plot analysis of magnetization data (Arrott [83]) of magnetization data.

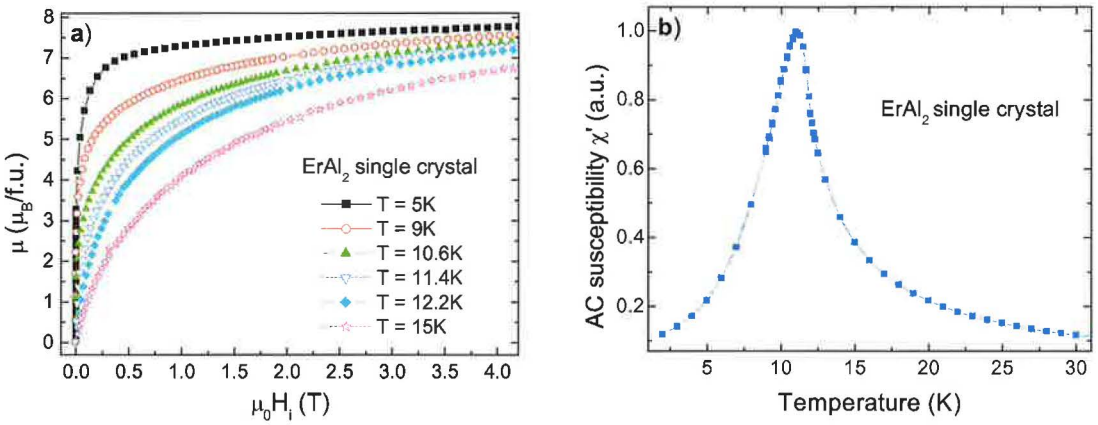

Figure 5.1 Magnetisation isotherms at selected temperatures around T_C (a) and real part of AC susceptibility (b) of $ErAl_2$ single crystal showing the transition T_C = 11K. Measured on sample in a straw.

5.1.2 Magnetic properties under hydrostatic pressure

Magnetic properties under applied hydrostatic pressure were measured at two values of pressure, 0.07 GPa and 0.6 GPa. The magnetization curve *M(H)* were measured at 2 K. The temperature dependent AC susceptibility $\chi(T)$ was measured from 30 K beyond the transition temperature.

The obtained results showed that the total magnetic moment (at 4 T) does not change in the used hydrostatic-pressure range. This supports well the expected scenario of behaviour of the well localized 4*f*-electron states of the Er^{3+} ions under a hydrostatic pressure. The 4*f*-electron states are well localized and also covered by 5*f*-electron states and so they are hard to influence by a pressure application. Further, the hydrostatic pressure causes the symmetric decreasing of lattice parameter of the cubic structure so it can be assumed that the surrounding of an erbium ion is not changed.

Data from the $\chi(T)$ measurements showed that the curves shift slightly towards higher temperatures with increasing hydrostatic pressure as expected for an 4*f*-electron ferr-magnet.

5.1.3 Magnetic properties under uniaxial pressure

Uniaxial-pressure experiments were done up to ~ 0.2 GPa. The magnetization as a function of magnetic field $M(H)$ was measured 5 K. The $\chi(T)$ dependence was measured in the same conditions as in hydrostatic pressure.

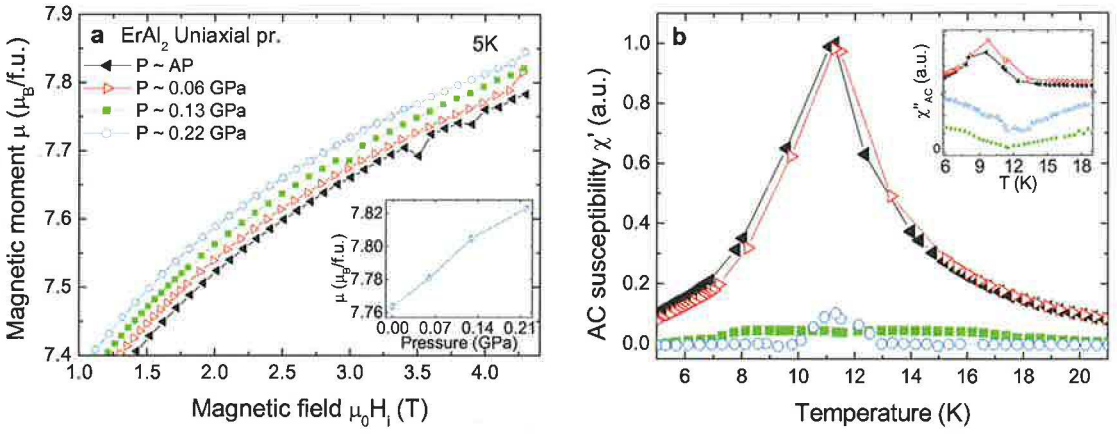

Figure 5.3 Field dependent magnetization at temperature 5K (a) and real part of AC susceptibility (b) of ErAl single crystal under various applied uniaxial pressure. The insets show a development of the total magnetic moment (at 4.5T) (a) and of the imaginary part of AC susceptibility (b) with applied pressure under same condition as the main graphs.

The Fig. 5.3a shows the obtained $M(H)$ results in decreasing field, confined for better resolution just on the region above 1T. It is seen that the total magnetic moment (at 4 T) increases continuously with increasing uniaxial pressure even the nominal values of the applied pressure are three times smaller than in case of hydrostatic pressure application. This can be explained so that by the uniaxial compression the changes in the lattice parameters are anisotropic. Consequently, the symmetry for the Er-ion neighbourhood is modified and the corresponding changes of crystal-field parameters may, in principle, yield an enhancement of the Er-magnetic moment. Further experimental and theoretical studies are desired to confirm this scenario.

Fig. 5.3b displays the data for $\chi'(T)$ and $\chi''(T)$ in the vicinity of the transition temperature. One can see that the uniaxial-pressure appliance up from 0.13 GPa causes a dramatic change in shape with respect to the original curve. This resembles the effect of DC magnetic field application observed by Levin et al. [24] who ascribed it to domain walls movements and domain magnetization rotations. It could mean that the domain structure present in the sample in the moment of uniaxial-pressure application changed dramatically. Obviously, it may be expected that the reduced symmetry of the crystal lattice induced by the uniaxial pressure leads to growth of certain domains on account of some other.

Chapter 6 Properties of $Er(Co_{1-x}Si_x)_2$ compounds with x = 0, 0.25

6.1 Results and discussion

6.1.1 Structure and composition analysis

The crystal structure of the prepared compounds of $ErCo_2$ and $Er(Co_{0.975}Si_{0.025})_2$ was characterized on powdered samples at room temperature by means of the X-ray powder diffraction analysis (see Fig. 6.1). Only the reflections corresponding to the expected cubic C15 Laves phase have been revealed. The refined values of the lattice parameters a = 714.4 pm and 715.5 pm for $ErCo_2$ and $Er(Co_{0.975}Si_{0.025})_2$, respectively, are in a good agreement with data in the literature (Cuong [84]; Daniš et al. [52]).
Homogeneity and stoichiometry of the prepared material was also proved on the Microprobe (see Fig. 6.2). From the qualitative point of view, both samples show the dominant desired matrix phase with tiny islands of spurious phases. The impurity phases are basically the Er metal, cobalt and erbium-oxides. The detailed concentration analysis was hampered by the fact that the involved low-energy Er- and Co-peaks, respectively, were influenced by a high background and the higher-energy peaks were considerably over-lapping which caused enhanced uncertainty in determining the concentrations and consequently the Er-concentration has been underestimated.

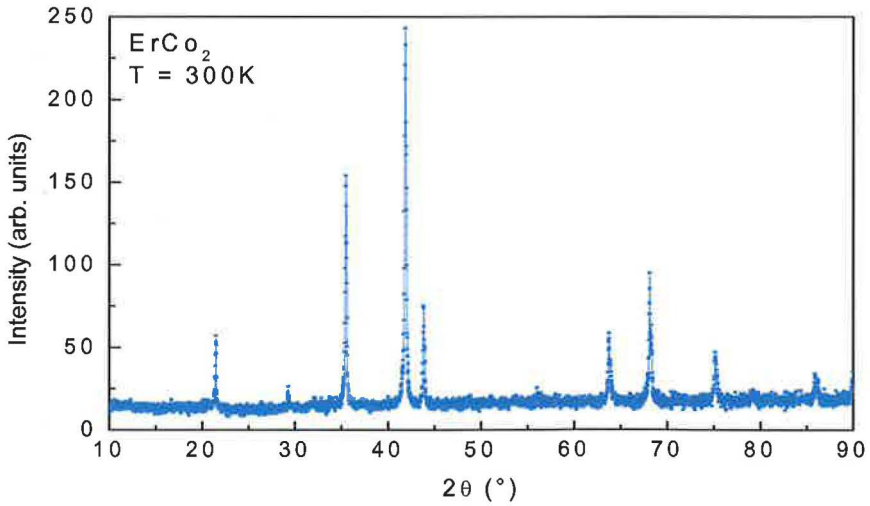

Figure 6.1 Observed diffraction pattern of $ErCo_2$

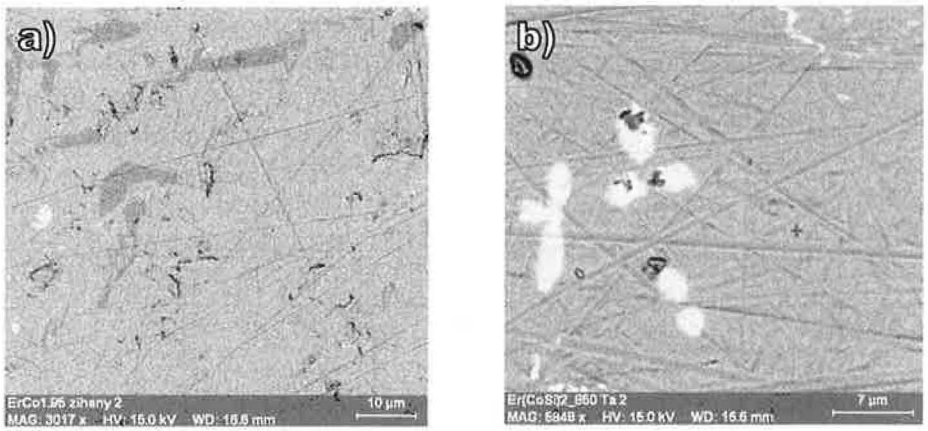

Figure 6.2 Pictures from SEM of $ErCo_2$ (a) and $Er(Co_{0.975}Si_{0.025})_2$ (b) compounds

6.1.2 Magnetization behaviour

Magnetization behaviour at ambient pressure

The temperature dependent magnetization measurements *M(T)* of the $ErCo_2$ and $Er(Co_{0.975}Si_{0.025})_2$ compounds at ambient pressure were performed under applied 0.1 T DC magnetic field up from 4 K. The observed transition temperatures T_C = 33 K and 42 K for $ErCo_2$ and $Er(Co_{0.975}Si_{0.025})_2$, respectively, are in a good agreement with literature (e.g. Syshchenko et al. [42]; Cuong et al. [84]). Abrupt changes at the T_C indicate the pronounced first-order transition.

The magnetization curves *M(H)* at ambient pressure were measured on free-powder samples at 2 K and around the transition temperature, from 28 K to 37 K with a 1K-step and from 35 K to 65 K with a 3K-step for $ErCo_2$ and $Er(Co_{0.975}Si_{0.025})_2$, respectively.
As for the 2K-magnetization curves, the measured total magnetic moment for $Er(Co_{0.975}Si_{0.025})_2$ is slightly higher than the one for $ErCo_2$. Because of comparing with the data in literature, two ways of analysing were used. The magnetization at 5 T is M_{5T} = 6.88 μ_B and 7.03 μ_B for the $ErCo_2$ and the $Er(Co_{0.975}Si_{0.025})_2$ compound, respectively. When using the law of approach to saturation (Cuong [84])

$$M(H) = M_S\left(1-\frac{A}{H}-\frac{B}{H^2}\right)+\chi H, \qquad (6.1)$$

where M_S is the saturated magnetization, A is parameter connected with magnetic inhomogeneities, B is parameter connected with magnetic anisotropy and χ is the high-field susceptibility. Then M_S = 7.11 μ_B and 7.19 μ_B for the $ErCo_2$ and the $Er(Co_{0.975}Si_{0.025})_2$ compound, respectively.

The Co-magnetic moment of our materials can be calculated from the total magnetic moments (presented higher) if we suppose the ordered Er moment μ_{Er} = 9 μ_B and antiparallel alignment of the Er and Co moments. The obtained values of Co-magnetic moment[11] decreases slightly from 0.95 μ_B to 0.91 μ_B for $ErCo_2$ and the $Er(Co_{0.975}Si_{0.025})_2$, respectively.

[11] Calculated from the M_S obtained from the low of approach of the saturation.

This is in contrast with the pronounced tendency (see further), nevertheless, taking into account the variability of the Co-moment values presented in literature (μ_{Co} = 0.9 – 1.07 μ_B and 1.13 μ_B for $ErCo_2$ [20, 21, 51, 68, 85] and for $Er(Co_{0.975}Si_{0.025})_2$ [20, 50, 51], respectively), the inconsistency can be tentatively accounted to differences in sample preparation.

Table 6.1 Observed changes in T_C and μ_{Co} for $RE(Co_{1-x}Si_x)_2$ system (RE = Er, Ho, Dy)

x	Er		Ho [b]		Dy [c]	
	T_C(K)	μ_{Co} (μ_B/at)[a]	T_C(K)	μ_{Co} (μ_B/at)	T_C(K)	μ_{Co} (μ_B/at)
0	32.6	1.07	78	1.00	142	1.0
0.025	44	1.13	95	1.03	142	1.15
0.500	54	1.20	112	1.06	148	1.20
0.725	64	1.00	115	1.05	146	1.18
0.100	68	0.88	112	0.88	146	1.08

[a]..Taken from Cuong et al. [51];
[b]..Taken from Duc et al. [86];

Table 6.2 Observed changes in T_C for $RE(Co_{1-x}Al_x)_2$ system (RE = Er, Ho, Dy)

x	Er	Ho	Dy
	T_C(K)	T_C(K)	T_C(K)
0	32.6	75	140
0.025	60	90	162
0.500	70	120	180
0.725	90	140	190
0.100	120	160	200

Taken from Duc et al. [87];

The experiments where one (or both) elements is substituted by some another one help us to improve knowledge about processes in the studied system and importance of particular interactions. It can be helpful to compare influence of substitution on similar systems. When substituting Si in the $RECo_2$ (RE = Er, Ho, Dy) the resulting tendency is similar – with increasing Si-amount (until a certain value; varying for individual RE) both the T_C and the induced Co-magnetic moment μ_{Co} increase (see Table 6.1); the enhancement of T_C is much milder than the one observed for Al-substitution (see Table 6.2). In (Y,Lu)Co_2 system, Al or Si substitution leads to an enhancement of the Co susceptibility and also an increase of the μ_{Co} (for low x-amounts) was affirmed (Duc et al. [86, 87]). It was also confirmed that Al or Si substitution causes decrease of critical field H_c (Murata et al. [88]).
One of the latest theoretical work (Khmelevskyi et al. [35]) dealing with the $RECo_2$ family pointed out that the Co-Co distance is one of the critical parameter for the Co-magnetic moment formation pointing on the compounds that have the largest lattice volume ($TbCo_2$ – $PrCo_2$, Gignoux et al. [7] and ref. therein) and that prove a stable Co magnetic moment even above the transition temperature. But when comparing the effects of Al and Si substitution that prove different influence on the room-temperature lattice parameter (increasing for Al and almost invariable for Si substitution[12]) we see that the lattice-parameter size cannot be

[12] This trend holds also for other compounds from the $RECo_2$ series (Duc et al. [20, 86, 89]; Cuong et al. [20]).

decisive. The changes that occur with additional substitution x are very complex. Firstly, with increasing x, the number of Co atoms per unit cell reduces (Cuong et al. [51, 84]). It changes the number of 3*d*-electrons and the nearest-neighbour Co-Co distance leading to an energetic shift of the bands and of the Fermi level and to an effective reduction of the overlap integral of 3*d* wave function and band narrowing. As a result, a full splitting of majority and minority subbands happens. Further, exchange interactions between Er- and Co-sublattice are changed which leads to a T_C-shift. Modification in the effects due to different substituents are associated with a different degree of the 3*d*-*p* hybridization (Aoki et al. [90], Duc et al. [86]).

Selected magnetization curves are presented in the Fig. 6.3a and 6.4a. It can be seen that the samples show the pronounced metamagnetic transition (MT) at temperatures T_C accompanied by hysteresis on the magnetic curves. Also with increasing temperature the critical field necessary for the MT increases and the magnetization step gradually diminishes. The metamagnetic behaviour is more evident from the S-shaped curves in Arrott plots in Fig. 6.3b and 6.4b.

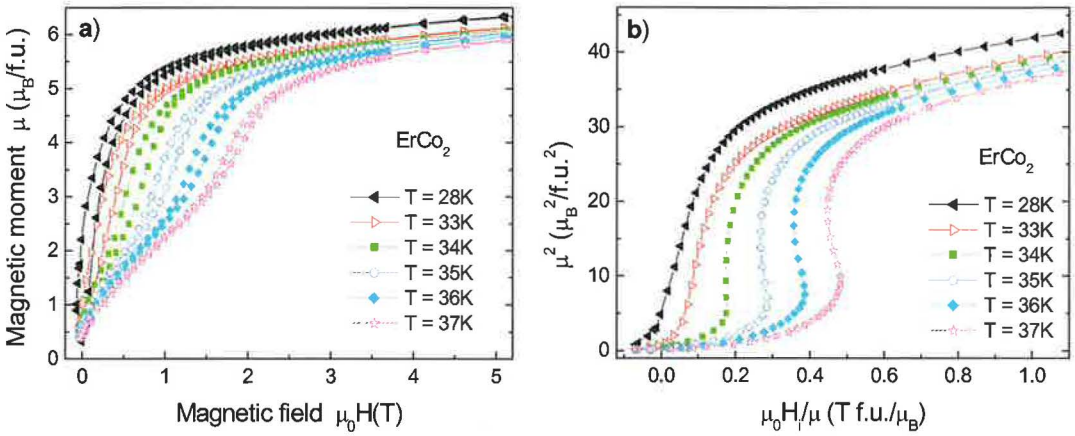

Figure 6.3 Magnetisation isotherms of $ErCo_2$ compound (a) and calculated Arrot plots (b) at several temperatures around the transition temperature showing the metamagnetic transition above the T_C = 33 K.

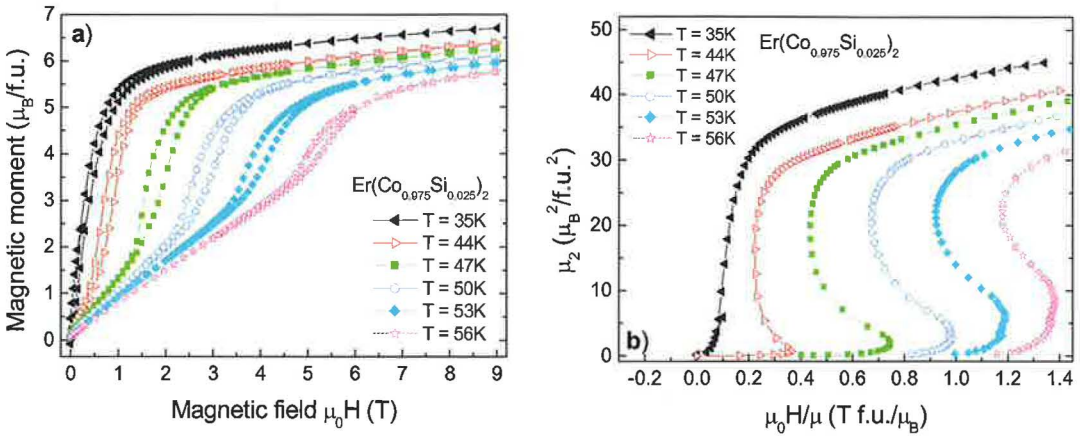

Figure 6.4 Magnetisation isotherms of $Er(Co_{0.975}Si_{0.025})_2$ compound (a) and calculated Arrot plots (b) at several temperatures around the transition temperature showing the metamagnetic transition above the T_C = 42 K.

Magnetization behaviour under pressure

Magnetization properties under applied hydrostatic pressure up to ~ 1 GPa were measured for exploring the development of the Co-magnetic moment. The experiments were performed in the appropriate hydrostatic CPC. (The given pressure values were determined at the Pb superconducting-transition temperature.)

Temperature dependent ZFC and FC magnetization measurements *M(T)* were performed in the temperature range 4 – 70 K during heating under 0.1 T applied DC magnetic field. In the Fig. 6.5 are presented the results for FC measurements. One can see that in both cases the transition temperature shifts towards lower temperatures with an increasing pressure. The same tendency approved also the ZFC curves. It is also interesting to inspect the *M(T)* dependences which clearly show already qualitative differences in the behaviour above T_C that allow us to suggest much weaker role of spin fluctuations in the Si-doped sample.

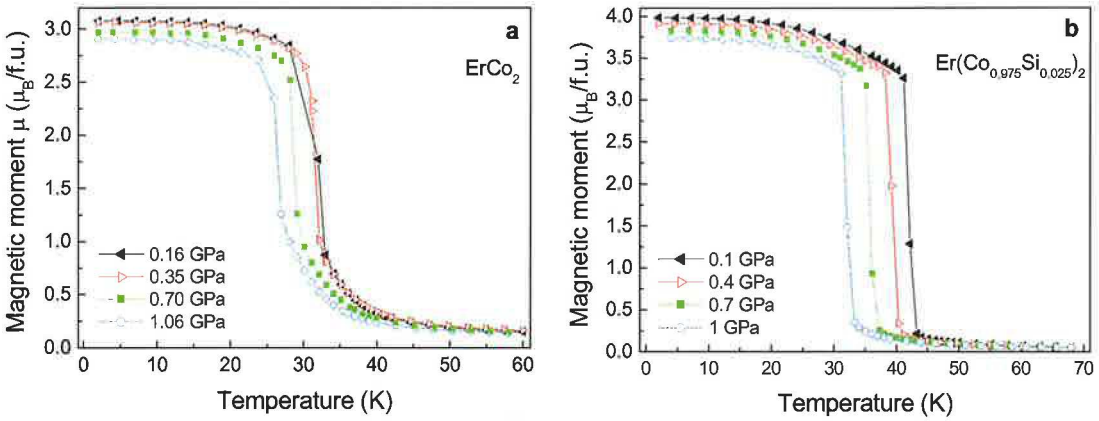

Figure 6.5 Temperature dependence of FC magnetization of $ErCo_2$ (a) and $Er(Co_{0.975}Si_{0.025})_2$ (b) under various applied hydrostatic pressure, in 0.1 T applied DC magnetic field. Given pressure values were determined at the Pb superconducting T_c.

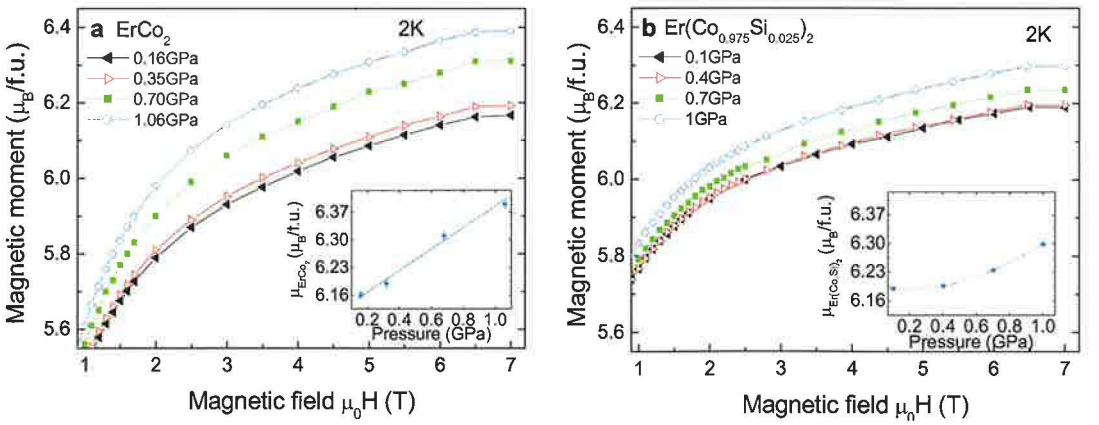

Figure 6.6 Field dependence magnetization of $ErCo_2$ (a) and $Er(Co_{0.975}Si_{0.025})_2$ (b) under various applied hydrostatic pressure, at temperature 2 K. The insets show the pressure dependency of total magnetic moments of the corresponding compounds. Given pressure values were determined at the Pb superconducting T_c

Magnetization curves *M(H)* were measured at 2 K in the field range 0 – 7 T during increasing

and decreasing of the applied field. The Fig. 6.6 displays the obtained results in decreasing field, confined for better resolution just on the region above 1 T. In both cases, the pressure application leads to an increase of the total magnetic moment in field of 7 T. At the first sight the magnetization in the Si-doped sample saturates much better which also points to a much smaller role of spin fluctuations in this material.
When supposing that the pressure has just a negligible influence on the rare-earth moment[13] then the change of the total magnetic moment μ with a pressure is given approximately by the change of the Co moment μ_{Co} with pressure. Then it means that the Co moment decreases with increasing pressure. This effect was confirmed earlier by Cuong et al. [51, 84] who studied the Co-moment formation under pressure also by means of magnetovolume effect and who observed reduction of the volume expansion with applied pressure.
For the $ErCo_2$ compound, the value of $\partial\mu_{Co}/\partial P \sim -\frac{1}{2}\,\partial\mu/\partial P = 0.0133$ μ_B/f.u. can be estimated from a roughly linear fit of the data (inset in Fig. 6.6a). As for the $Er(Co_{0.975}Si_{0.025})_2$ compound, the pressure derivatives (see inset in Fig. 6.6b) of the Co moment are considerably smaller (and the $\mu_{Co}(P)$ development is not linear) which also points to higher stability of the Co-magnetic moment (reduced role of spin fluctuations) caused by the Si-substitution.

6.1.4 AC susceptibility behaviour

AC susceptibility behaviour at ambient pressure

The AC susceptibility measurements χ_{AC} of both the $ErCo_2$ and the $Er(Co_{0.975}Si_{0.025})_2$ compounds were performed in the range 300 – 2 K, in various applied DC magnetic fields and at various excitation frequencies from 10 – 10000 Hz. Examples of obtained data are in Fig. 6.7a-d. The results are in a good agreement with the data in literature (see e.g. Herrero et al. [60-62]; Cuong et al. [50, 84]; Oner et al. [91]; Prokleska [92]).

$ErCo_2$

As for the $ErCo_2$, the real part of AC susceptibility data $\chi'(T)$ shows a sharp peak at T_C (= 33 K) followed by a paramagnetic decay at higher temperatures. The $\chi''(T)$ data also coincides T_C in this case. The T_C value determined from AC susceptibility data is in a good agreement with the transition temperature determined from the magnetisation and resistivity measurements. At lower temperatures, the $\chi'(T)$ dependence shows a shoulder around 20 K that coincides with a broad maximum on the $\chi''(T)$ curve[14] whereas no anomaly of this kind is seen in AC susceptibilities measured on the Si doped sample. Also this difference between magnetic behaviour of $ErCo_2$ and $Er(Co_{0.975}Si_{0.025})_2$ can be understood within the scenario considering dramatic change in the role of spin fluctuations connected with Si substitution for Co.
The paramagnetic $1/\chi'(T)$ data are linear except for the deviation around 100 K (inset in Fig. 6.7b) which is in agreement with the results of Herrero et al. [60-62] ascribed by these authors to the flipping of the Co moments at $T_F \sim 100$ K. In the $\chi'(T)$ data, this anomaly is less visible. It is clearly more evident in the $1/\chi'(T)$ data and the corresponding susceptibility contribution can be separated from nearly linear dependence in the immediate surrounding. In the imaginary part $\chi''(T)$ data, the anomaly position can be determined just at frequency

[13] The 4f-electron states are well localized and consequently the value of the Er magnetic moment is intact by pressure-induced variations of interatomic distances.
[14] This was already pointed out by Oner et al. [91] but without explanation.

f = 10 kHz, at lower frequencies the data are very noised and cannot be used – see Fig. 6.7b. Nevertheless, the high frequency curve does not prove peak-like-shape as presented in the Herrero et al.-results. In our case appearance of the anomaly can be attributed with the step-decreased value of $\chi''(T)$ with increasing temperature – see the inset in Fig. 6.7b.

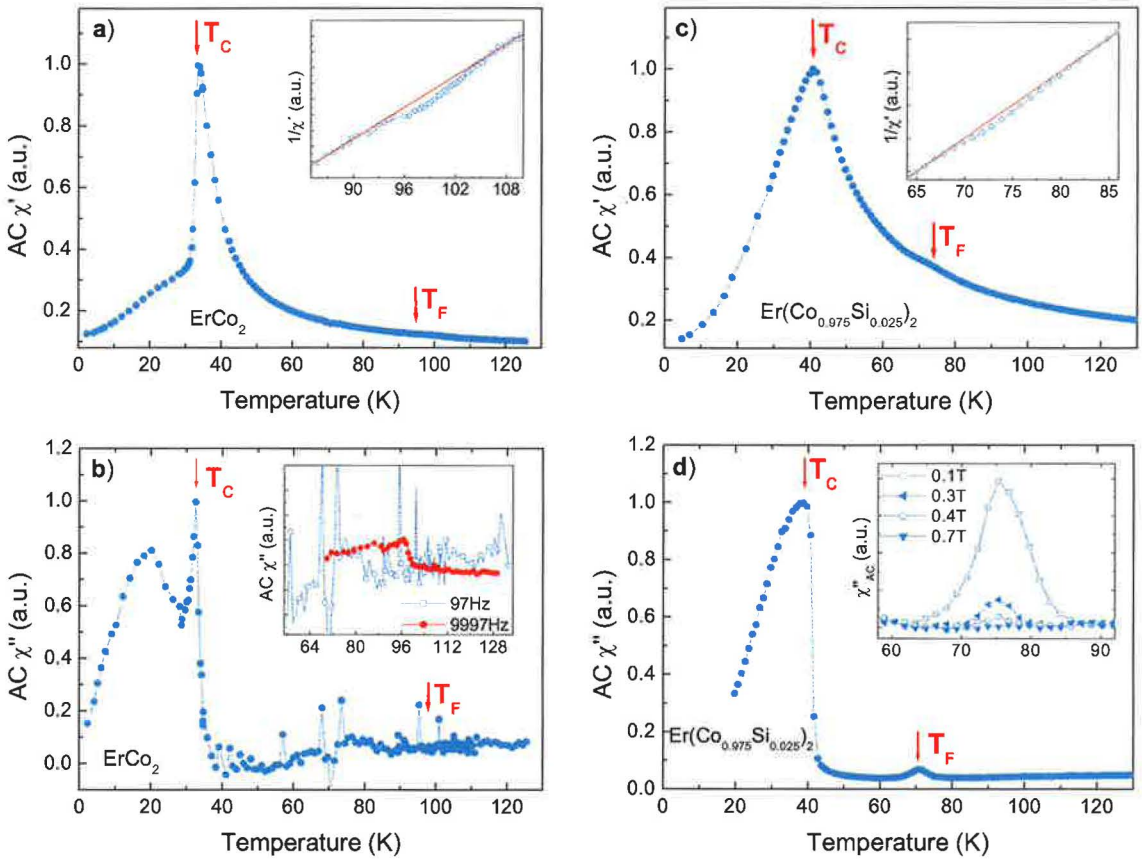

Figure 6.7 Temperature dependence of real and imaginary parts of AC susceptibility of $ErCo_2$ (a, b) and $Er(Co_{0.975}Si_{0.025})_2$ (c, d) measured at zero magnetic field and ambient pressure during cooling. The insets show in detail the observed anomalies in $1/\chi'(T)$ data (a) and (c), that have same character by both compounds, and in $\chi''(T)$ data, that are different.

$Er(Co_{0.975}Si_{0.025})_2$

Also here the temperature dependence of the real part of AC susceptibility data $\chi'(T)$ shows a peak at the T_C (= 42 K) followed by a paramagnetic decay at higher temperatures (Fig. 6.7c). In comparison with $ErCo_2$, the peak is rather smooth, nevertheless it also coincides with the temperature of the maximum value of $\chi''(T)$.

Also in this compound, an anomaly in the paramagnetic phase was discovered at $T_F \sim 70$ K that is shifted to lower temperatures in comparison with the $ErCo_2$ compound. The observed anomaly was very strong in the $\chi''(T)$ data even at low frequencies. The anomaly was studied in detail as a function of the excitation frequency and magnetic field. It is clearly observed that the peak is suppressed by the field of 0.7 T (see the inset in Fig. 6.7d). Within the frame of accuracy of our data it was not possible to determine any shift connected with frequency and field change as was presented by Herrero et al. [60-62].

These two magnetic phenomena characteristic for $ErCo_2$ (and $Er(Co_{0.975}Si_{0.025})_2$), the critical

temperature T_C and the flipping temperature T_F, respectively, must be intimately connected with the electronic structure and exchange interactions. Knowing the composition and crystal structure one may consider two sublattices - the Er and Co one - and consequently the Er-Er and Co-Co intrasublattice exchange interactions and Er-Co intersublattice exchange interactions are in the game.
Herrero et al. [62] suggest that the anomaly at T_F is connected with the fact that the Er and Co moments (!) would like to align antiparallel to each other (Er-Co interaction) but due to a strong Co-Co interaction an individual flipping of the Co is not possible and it is necessary that this happens in a collective way – in the clusters. If the Co-magnetic moments were really stable at high temperatures like the Fe moments in $REFe_2$ the direct Co intrasublattice exchange interactions would lead to ferromagnetic ordering also in YCo_2 and $LuCo_2$ and the T_C value of $ErCo_2$ would be much higher than the T_C actual value.
As for the T_C, the accepted scenario (Syshchenko et al. [45]) suppose that the 3*d*-states of Co hybridize with the 5*d*-states of Er which gives rise to the indirect exchange interaction with the 4*f*-electron magnetic moments of the Er ions. This interaction is apparently enhanced when *p*-electrons are brought by the substitution of Si atoms in the Co sublattice which is manifested by the considerably increased T_C value of the $Er(Co_{0.975}Si_{0.025})_2$ with respect to the T_C of $ErCo_2$.
As observed, the effect on T_F with Si-substitution is opposite (T_F decreases) which leads us to assume that the "ferromagnetic" clustering of Co-magnetic moment, or rather their precursors, in the paramagnetic range must be driven also by the Co intrasublattice exchange interaction. Further details of physics around the T_F concerning detailed determination of clustering process may be unambiguously discussed only after relevant microscopic experiments (neutron scattering, XMCD, μSR) are done in future.

AC susceptibility behaviour under pressure

The temperature dependent AC-susceptibility measurements $\chi(T)$ under hydrostatic pressure of $ErCo_2$ and $Er(Co_{0.975}Si_{0.025})_2$ were performed in the temperature range from 120 K down beyond the transition temperature. On each compound, two series of measurements were done – the first one in the CPC designed for the SQUID magnetometer, the second one in CPC for the PPMS instrument employing a special coil.

$ErCo_2$

In Fig. 6.8a,c are shown the results in the temperature region around the transition temperature T_C. One can see that the AC-susceptibility curve changes significantly its character under pressure – it changes the position, width and amplitude.
For practical reasons we will associate here the transition temperature with the maximum of the derivative of $\partial\chi'/\partial T$ (Fig. 6.8b,d) which allows us to determine reasonably e.g. splitting of the transition temperature of the Er and Co sublattice[15], respectively. From the evolution of the χ' vs. T and $\partial\chi'/\partial T$ vs. T curves one may deduce that the T_C decreases initially linearly up to approximately 1.4 GPa, varying with $\partial T_C/\partial P = -6.6 \pm 0.2$ K.GPa^{-1}. The measurements under pressures beyond ~ 1.7 GPa prove clearly appearance of two partially overlapped $\chi'(T)$ maxima. This should be the behaviour predicted by Hauser et al. [36] when the two

[15] We are aware a of certain inconsistency in comparison with determination of T_C in the previous chapter where the value of the T_C has been taken as the temperature of the $\chi'(T)$ maximum.

separate magnetic phase transitions are present – the lower, first-order-transition [16] temperatures corresponding with T_C^{Co} and the higher, second- order-transition temperatures corresponding with T_C^{Er}. Up to 2.4 GPa, the T_C^{Co}-branch development continues in the linear tendency of the T_C but the T_C^{Er} branch deviates, varying as $\partial T_C^{Er}/\partial P = -2.9 \pm 0.1$ K.GPa^{-1}, if roughly estimated with a linear tendency. Summarizing results are shown in the phase diagram T_C vs. P in the Fig. 6.9.

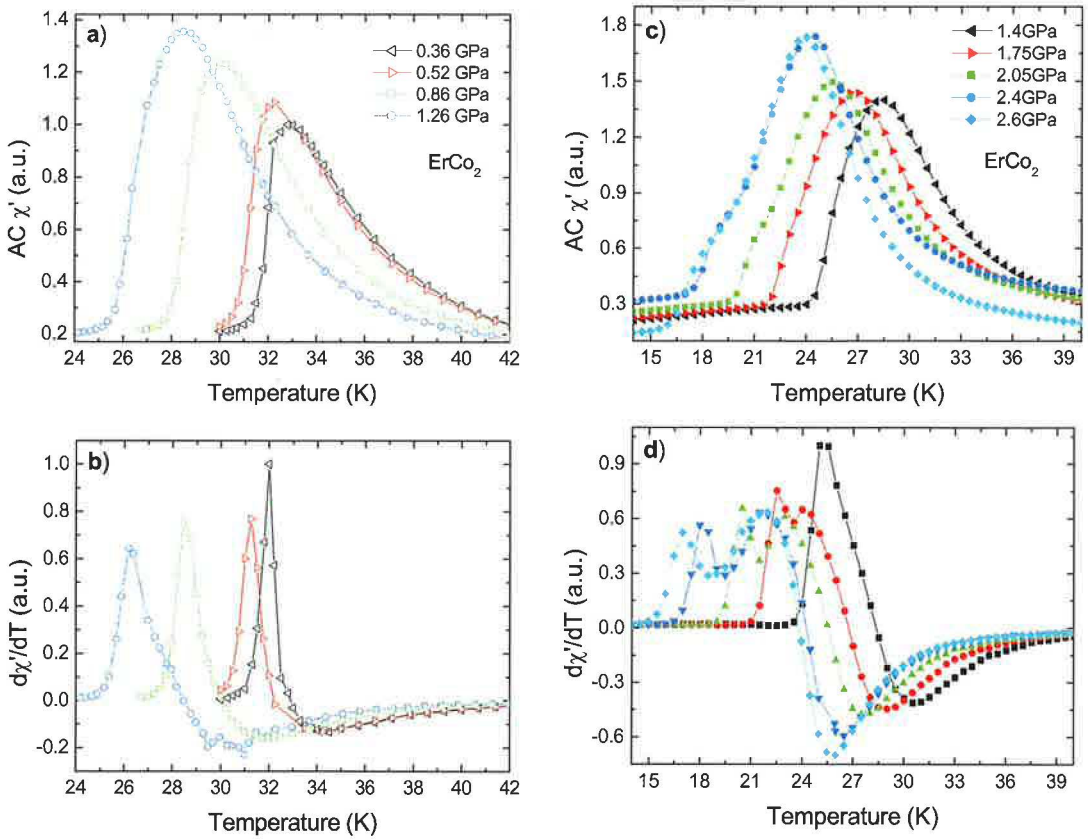

Figure 6.8 The temperature dependence of real part of AC susceptibility and the corresponding temperature derivations of $ErCo_2$ compound under various hydrostatic pressures taken in the CPC for the SQUID magnetometer (a,b) and in the CPC for the PPMS instrument with a special coil (c,d). The amplitudes of $\chi'(T)$ are normalized with respect to curve under the lowest pressure. The denoted pressure values were determined at room temperature. The data-point symbols in plots b and d correspond to same pressure as in plots a and c, respectively.

For approving the scenario of the splitting of the T_C in T_C^{Co} and T_C^{Er}, the $\chi'(T)$ data were fitted so that it was assumed that the measured curves are a convolution of two curves representing the Er and Co magnetic-moment behaviour, respectively. The highest-pressure curves were successfully fitted with two Gauss curves moving apart each other with increasing pressure. An example is showed in Fig. 6.10.

[16] The scenario introduced by Hauser et al. is based on considering the Co sublattice ordering at lower temperature than ordering of the Er sublattice when the conditions for metamagnetism in the Co sublattice are modified by sufficient external pressure.

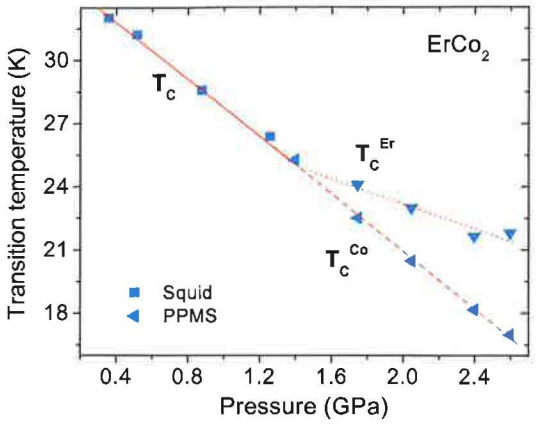

Figure 6.9 Phase diagram of transition temperature vs. hydrostatic pressure of $ErCo_2$ focused on the temperature region around the transition temperature. Both sets of measurements are included. One can clearly see the predicted (Hauser et al. [36]) transition-temperature splitting at ~ 1.4GPa. The red lines show estimated linear fits of the data. The denoted pressure values were determined at room temperature.

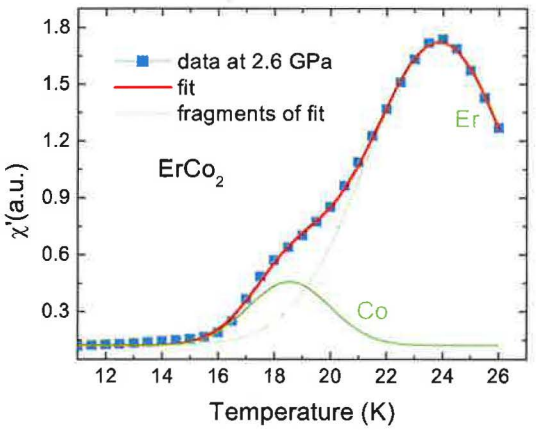

Figure 6.10 Fit (red line) of measured $\chi'(T)$ data of $ErCo_2$ (■) with two Gauss-type curves (green lines). Peak positions of fitted curves and their derivations are in a good agreement with the experimentaly obtained data.

In Fig. 6.11a are shown the results of $ErCo_2$ compound for temperature region around the flipping temperature T_F. (Herrero et al. [60-62]). For easier analysis the data were processed as followed: the original data $\chi'(T)$ were inverted into $1/\chi'(T)$, the anomaly was subtracted supposing that the purely paramagnetic data would follow the Curie-Weiss law (linear temperature dependency - at least in the nearest vicinity of the T_F); the final data were taken in absolute values. It can be clearly seen that the curves shift towards lower temperatures with increasing pressure.

Further, the temperatures maxima of such derived curves, were taken for a rough analysis as the comparative value of the T_F. However, because of noised data, these were sometimes not definite and so just for better clarity the curves were also fitted by a Lorenz function. The Fig. 6.11b shows a phase diagram T_F vs. P. As for the fitted data, each set of measurements shows roughly a linear tendency but shifted from each other. This could be most probably attributed to differences in each set of measurements (due to differences between used instruments).

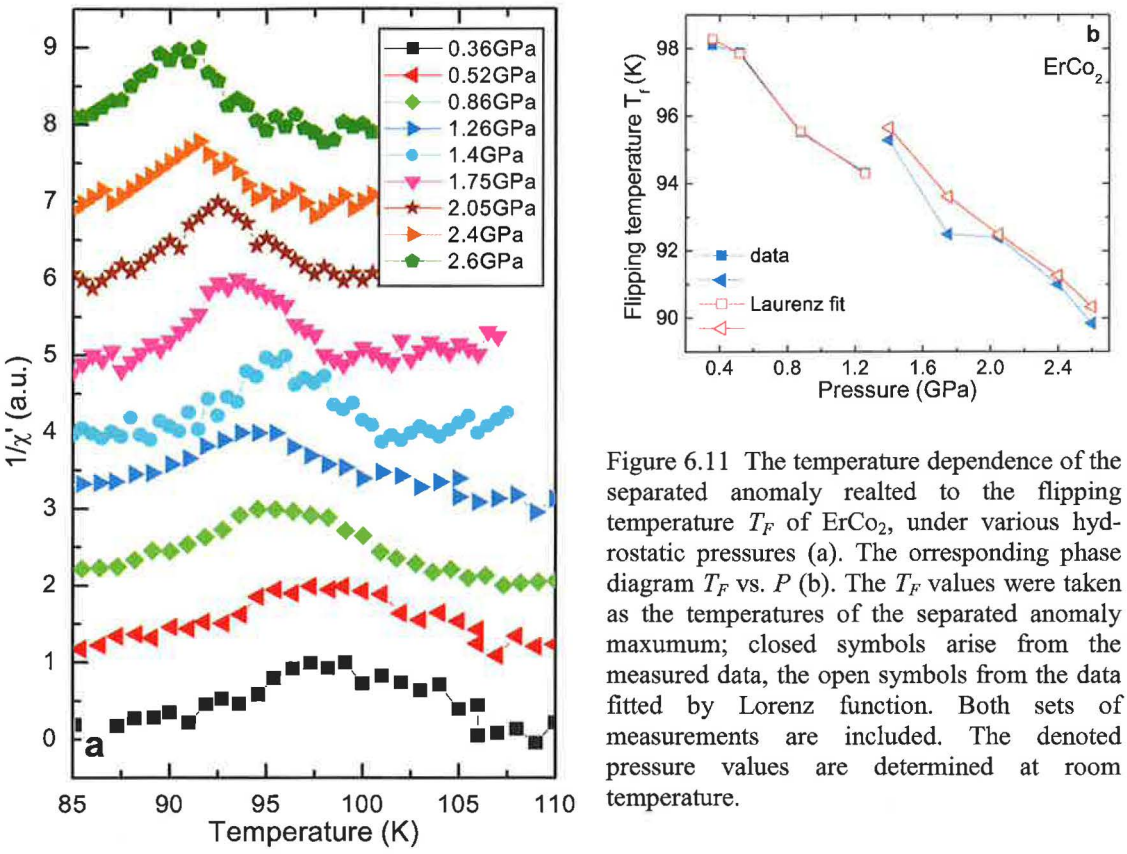

Figure 6.11 The temperature dependence of the separated anomaly realted to the flipping temperature T_F of $ErCo_2$, under various hydrostatic pressures (a). The orresponding phase diagram T_F vs. P (b). The T_F values were taken as the temperatures of the separated anomaly maxumum; closed symbols arise from the measured data, the open symbols from the data fitted by Lorenz function. Both sets of measurements are included. The denoted pressure values are determined at room temperature.

$Er(Co_{0.975}Si_{0.025})_2$

In the Fig. 6.12 are presented selected $\chi'(T)$ curves in the temperature region around the transition temperature. One can see that also for this compound the $\chi'(T)$ behaviour is considerably influenced by applying external hydrostatic pressure.

In comparison with the parent compound ($ErCo_2$), the amplitude of the $\chi'(T)$ increases gradually at a high rate for pressures up to 2.6 GPa where it reaches almost 20times higher value than at ambient pressure. Beyond 2.6 GPa, the amplitude does not increase anymore, nevertheless the $\chi'(T)$ peak becomes broader. The splitting of the Er- and Co-sublattice, respectively, ordering temperatures observed for $ErCo_2$ is not evident in the case of $Er(Co_{1-x}Si_x)_2$ at available pressures although the gradual broadening of the $\chi'(T)$ beyond 2.6 GPa maybe considered as a precursor of such splitting. Measurements at higher pressures are desired to confirm whether the T_C splitting appears also here. As for the development of the transition-temperature with pressure, T_C vs. P (where the T_C is determined from the maxima of the $\partial\chi'/\partial T$), the T_C decreases up to 1.7 GPa, varying as $\partial T_C/\partial P = -9.4 \pm 0.8$ K.GPa^{-1}, if roughly approximated with a linear dependency. Around 1.7 GPa, the de- pendency deviates and varies approximately as $\partial T_C/\partial P = -3.0 \pm 0.4$ K.GPa^{-1}.

As for the pronounced anomaly around T_F, this was observed only up to pressure 1.2 GPa. The corresponding phase diagram is presented in Fig. 6.13. With increasing pressure, the character of the inverse $\chi'(T)$ gets more deviated from an ideal linear dependency and it is not possible to separate the anomaly. So it cannot be excluded that the anomaly does not disappears at higher pressures.

Summarizing, from our measurements around the T_F follows that a pressure application has a similar influence on the flipping-temperature development as the applied magnetic field has (Herrero et al. [60-62]). For reminding, the flipping of the orientation of a Co moment happens in a collective way in clusters because it is energetically favorable. During the flipping process the Co-Co exchange interaction should be overcome and the clustering allows minimizing the number of antiparallel Co-Co neighbours. The pressure application leads to decreasing Co-Co distances and consequently an enhanced overlap of 3*d*-wave functions of neighbouring Co atoms that on one side may enhance the exchange interaction in the Co sublattice but on the other hand the 3d electrons become more delocalized and the Co magnetic moment further suppressed. Which of the two effects becomes dominant cannot be answered at this stage of understanding.

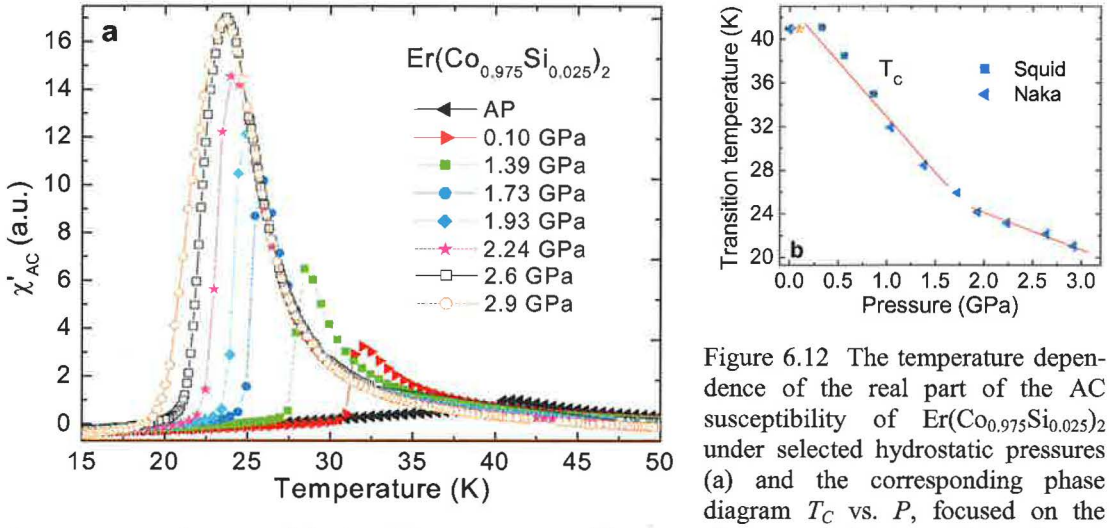

Figure 6.12 The temperature dependence of the real part of the AC susceptibility of $Er(Co_{0.975}Si_{0.025})_2$ under selected hydrostatic pressures (a) and the corresponding phase diagram T_C vs. P, focused on the temperature region around the transition temperature. The denoted pressure values were determined at room temperature. Taken in the CPC designed for the PPMS instrument with the special coil.

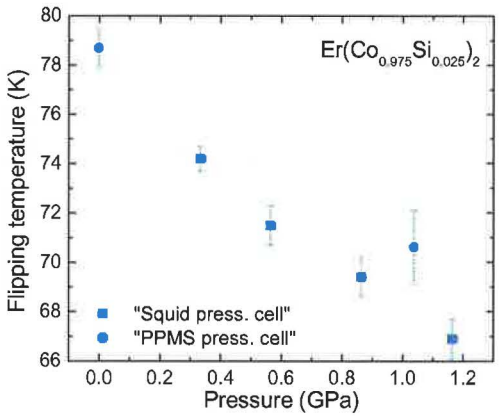

Figure 6.13 Phase diagram T_F vs. P of $Er(Co_{0.975}Si_{0.025})_2$ focused on the temperature region around the anomaly. The T_F values were taken at the maximal values of the separated anomalies. Both sets of measurements are included. The pressure values denoted were determined for the room temperature.

6.1.2 Electrical resistivity behaviour

Electrical resistivity behaviour at ambient pressure

The temperature dependencies of the electrical resistivity $\rho(T)$ of $ErCo_2$ and $Er(Co_{0.975}Si_{0.025})_2$ compounds at ambient pressure are shown in Fig. 6.14 a, b. The data are in

a good agreement with those reported earlier (Cuong et al. [50, 51]; Hauser et al. [36, 93]; Daniš et al. [52]). Both curves show the pronounced first-order magnetic phase transition at the Curie temperature T_C clearly approved by the step-like resistivity drop ascribed to the Co 3*d*-moment formation (Syshchenko et al. [44, 45]) and by a hysteresis in temperature. Both curves show a tendency to saturate with increasing temperature that was attributed to the spin-fluctuation scattering of the 3*d*-band (Baranov et al. [32]). In the case of $ErCo_2$, there is a characteristic anomaly in the vicinity of the transition temperature – an enhancement of resistivity when approaching T_C from higher temperatures - which has been ascribed to the critical conduction-electron scattering on spin fluctuations in the itinerant *d*-band (Syshchenko et al. [44, 45]).

With the Si-substitution, the T_C shifts to higher temperatures and the anomaly disappears (where the transition temperature T_C was determined as the maximum point of the $\partial\rho/T\partial$ curve). The residual (ρ_0) increases considerably with the Si-substitution for Co and that is an obvious consequence of the substitutional disorder in the Co sublattice.

The near-above-T_C anomaly characteristic for resistivity data of the parent compound is missing in data obtained for the Si-substituted sample. This result further corroborates the scenario of the diminished role of spin fluctuations that has been deduced already from magnetization and AC susceptibility behaviour of the Si-doped sample as discussed in previous chapters.

The phenomena connected with Co-moment flipping are not reflected in the resistivity data in the vicinity of the corresponding T_F neither for $ErCo_2$ nor for $Er(Co_{0.975}Si_{0.025})_2$ within the sensitivity and accuracy of our measurement. The effect of the Co-moment flipping is very subtle and consequently it is hidden in the sea of conduction-electron scattering on spin-fluctuation events in the paramagnetic range.

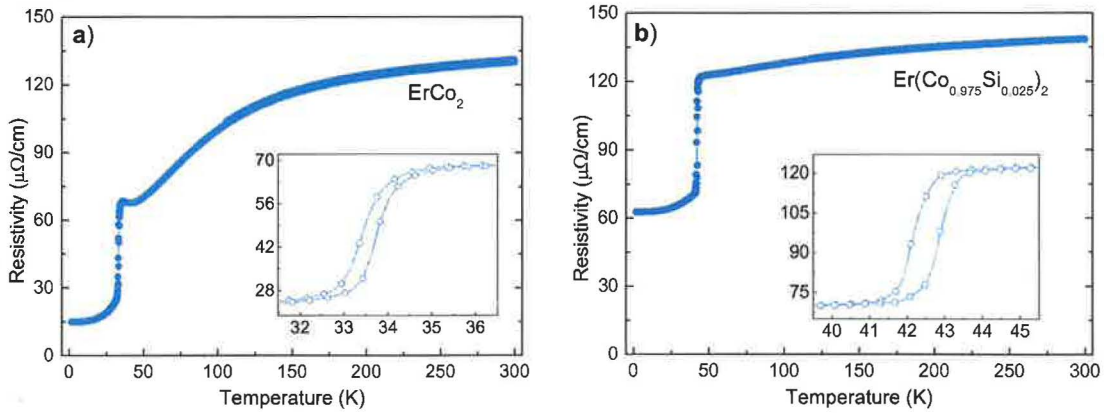

Figure 6.14 Temperature dependence of electrical resistivity of $ErCo_2$ (a) and $Er(Co_{0.975}Si_{0.025})_2$ (b) compounds measured in zero applied magnetic field and at ambient pressure. Both samples show a step-like resistivity drop approving the first order phase-transition.

Electrical resistivity behaviour under pressure

The temperature dependences of the electrical resistivity of $ErCo_2$ and $Er(Co_{0.975}Si_{0.025})_2$ under applied hydrostatic pressure were measured in the clamped pressure cell up to 3 GPa and in the Bridgman-type cell up to 8 GPa. The experiments in higher pressures for $Er(Co_{0.975}Si_{0.025})_2$ were in progress in the time of finalizing this thesis and the results are therefore not included.

$ErCo_2$

The electrical-resistivity measurements $\rho(T)$ of $ErCo_2$ under hydrostatic pressure were performed up to 8 GPa The obtained results up to 3 GPa (Fig. 6.15a) are in a very good agreement with literature data (Hauser et al. [36, 93]; Syshchenko et al. [42, 44, 45]). The experiments in higher pressures were affected with inappropriate shape of the sample and its location (Fig. 4.6b) which led to a non-hydrostatic spread pressure in the measured part (Eremets [81]; Hauser et al. [36]). The character of the curves roughly corresponds to the expected behaviour presented in literature (Syshchenko et al.[42, 44, 45]).

The measured data (Fig 6.15a) clearly reveal that the pressure affects significantly the resistivity behaviour. The magnetic ordering transition temperature decreases with increasing pressure and beyond 1.6 GPa the anomaly related with T_C considerably changes its character, so that actually it is difficult to decide whether and where the transition happens and of which type it is. Nevertheless, for quantitative treatment, (as for the ambient case) the maximum point of temperature derivative of the resistivity-curve $\partial\ \rho/\partial T$ is taken as the transition temperature T_C. From the T_C vs. P dependency (Fig. 6.15b,■) one can see that the T_C decreases with increasing pressure linearly up to 2.46 GPa, varying with $\partial T_C/\partial p$ = -(6.96 ± 0.30) K.GPa^{-1}. Probably beyond 2.9 GPa, the dependency would deviate from the original linear one and level off towards a pressure independent value as demonstrated by the experiments performed by Syshchenko et al. [42, 44, 45].

Further, the original anomaly in the T_C-vicinity becomes gradually enhanced with increasing pressure up to 3 GPa. The residual resistivity value remains almost intact.

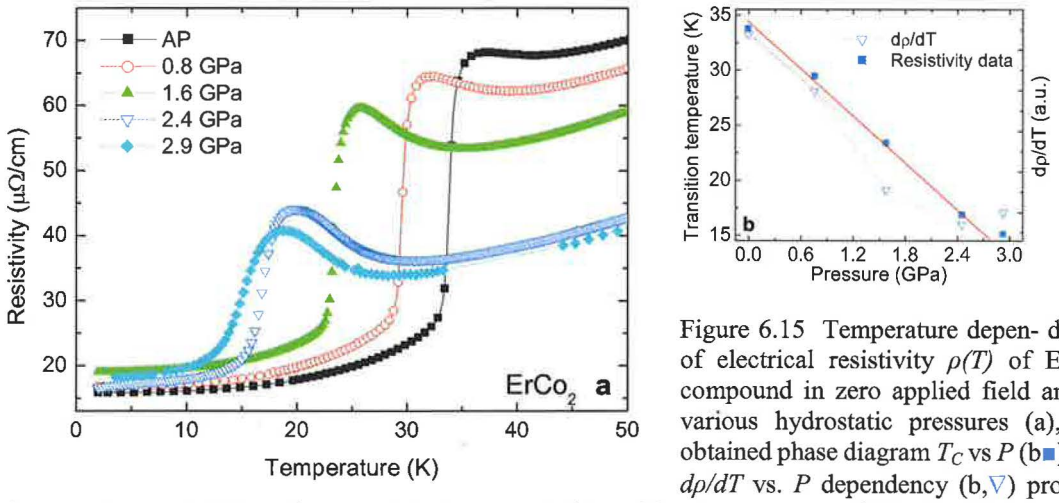

Figure 6.15 Temperature depen- dence of electrical resistivity $\rho(T)$ of $ErCo_2$ compound in zero applied field and at various hydrostatic pressures (a), the obtained phase diagram T_C vs P (b■) and $d\rho/dT$ vs. P dependency (b,▽) proving the range 0.8 – 1.6 GPa as the one where the expected transition- temperature splitting happens.

The values of the transition temperature obtained at various pressures correspond perfectly to the transition temperature T_C and further to the T_C^{Co} determined from the AC-susceptibility measurements but no evident transition-temperature splitting is observed. Further analysis is needed that would ascertain the splitting even from the resistivity data. Hauser et al. [36] used for indicating the temperature derivative of the resistivity pointing on the appearance of the minimum in these curves. Nevertheless, some minimum is always present even at ambient condition following from the character of the transition-temperature vicinity. When analysing the relative amplitudes of these features, we can see that the starting tendency of the data at lower pressures deviates at the 1.6 GPa (Fig. 6.16b,▽). So it can be roughly estimated that a change happens between the pressures 0.8 and 1.6 GPa. This range would be

in a good agreement with the results obtained from the AC-susceptibility measurements. Recently, Ishimatsu et al. [68] studied pressure influence (up to 4.2 GPa) by means of XMCD and X-ray Absorption Spectroscopy and discovered that the system develops through different magnetic regimes depending on the value of applied pressure. They observed significant changes in measured spectra above 1 GPa and concluded that the density of empty electronic states above the Fermi level decreases and also the Fermi level shifts. Further, they showed that a pressure increase leads to the 5*d*-electron-state localization resulting in decreased 3*d*-5*d* hybridisation. They also confirmed increased electronic perturbation with applied pressure. For $P \geq 3$GPa they observed unaltered spectra. The boundary-pressure values suggested by them are in very good agreement with the ones confirmed by our experiments.

The scenario of processes in the $ErCo_2$ can be following: At ambient pressure, the system orders at T_C owing to sufficiently strong exchange field able to split the 3*d* majority and minority subbands; the exchange field acts on the 3*d*-electron band via 3*d*-5*d* hybridisation. The scattering on spin fluctuations, present in the paramagnetic phase and demonstrated by anomaly enhancement near the T_C, is suppressed abruptly as the spin fluctuations are quenched. A pressure application causes the 3*d*-electron-band broadening, consequently their incomplete splitting and lower induced Co-magnetic moment. Increase of the pressure leads to increasing of the critical field H_c necessary to the metamagnetic transition of the Co moment approved as decrease of the T_C. Also the spin-fluctuation enhancement gets still stronger until the critical pressure $P_c \sim 1.6$ GPa. At P_c, the 3*d*-5*d* hybridisation is disturbed and so the Co moments do not order at the same moment as the Er ones. Above 3 GPa, the electronic structure probably stabilizes which is supported also by almost disappearance of the spin fluctuations. The induced Co-magnetic moment should finally disappear at ~ 4GPa (Hauser et al. [36]; Syshchenko et al. [45]).

$Er(Co_{0.975}Si_{0.025})_2$

In Fig. 6.16a $\rho(T)$ curves are presented for several values of hydrostatic-pressure appliance. The obtained results in low pressures are in a good agreement with literature (Cuong et al. [50, 51, 84]). It can be seen from the measured data that the character of the curves is just very slightly affected by the pressure.

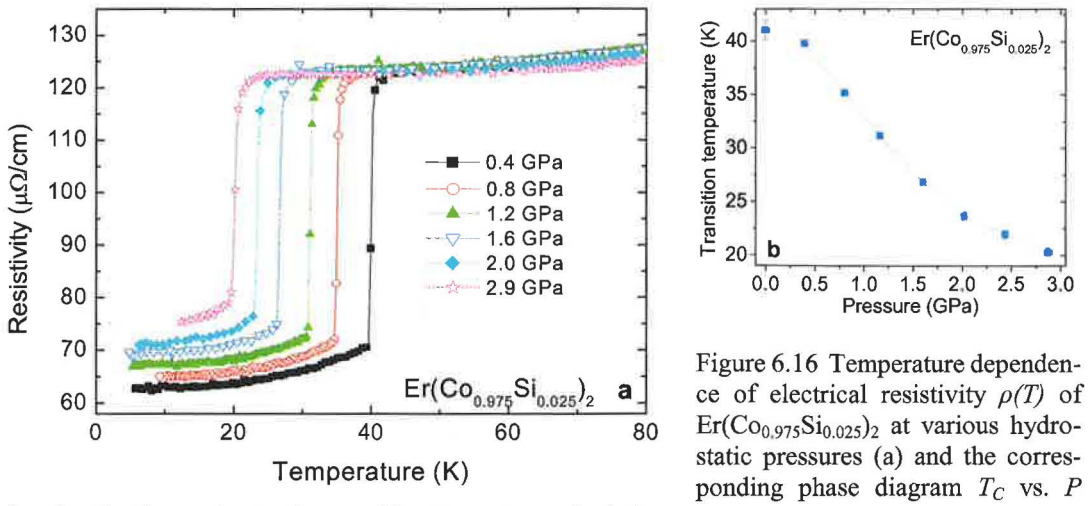

Figure 6.16 Temperature dependence of electrical resistivity $\rho(T)$ of $Er(Co_{0.975}Si_{0.025})_2$ at various hydrostatic pressures (a) and the corresponding phase diagram T_C vs. P showing the decreasing tendency without any strong deviation.

Within the entire pressure range of our experiment, no dramatic changes were observed. The

transition temperature T_C (determined from $\partial\rho/\partial T$-curve) decreases continuously with increasing applied pressure as shown in Fig. 6.16b. For all pressures, the resistivity curves prove a discontinuous change at the T_C, corroborating the original conclusion on the first-order-type transition. Further, the high-temperature resistivity under pressure keeps not only a similar character but even the absolute value as to the unpressurized sample. The residual resistivity ρ_0, on the other hand, increases continuously with increasing pressure, which contrasts to the ρ_0-behaviour of $ErCo_2$.
The near-above-T_C anomaly observed for $ErCo_2$, but missing in ambient-pressure data measured on $Er(Co_{0.975}Si_{0.025})_2$, has not emerged when the sample was under pressures up to 3 GPa. This points to the better stability of the Co-magnetic moment owing to the Si-substitutions for Co.
As expected, no indication of the Co-moment flipping in the vicinity of the corresponding T_F neither for $ErCo_2$ nor for $Er(Co_{0.975}Si_{0.025})_2$ has been observed in the resistivity data even in pressures up to 3 GPa.

6.2 Conclusions

In conclusion, we have prepared polycrystalline samples of $ErCo_2$ and $Er(Co_{0.975}Si_{0.025})_2$, characterized the crystal structure (the cubic Laves phase in both cases) by X-ray powder diffraction and composition by EDX microprobe.
For these materials we measured temperature dependencies of the electrical resistivity and AC susceptibility, and the magnetization curves at representative temperatures. All the measurements were done at ambient and high hydrostatic pressure in order to study impact of changes of interatomic distances on the main magnetic characteristics.
We have observed the influence of the Si substitution and application of pressure on the Co magnetic moment, Curie temperature T_C and the flipping temperature T_F and tried to formulate a scenario of physics of $ErCo_2$ considering variations of electronic structure and exchange interactions.

1. Low pressures (up to 2-3 GPa) lead to strong destabilization of the system in the vicinity of the transition temperature proved by enhancement of the spin fluctuations and splitting of the transition temperature. At high pressures the system is stabilized proved by re-decrease of the spin fluctuations and almost pressure independent transition temperatures of Er- and Co-magnetic sublattice.
2. With Si substitution the lattice parameter remain unaltered but Er- and Co-sublattice exchange interactions are changed leading to higher ordering temperature. The substituted system is stabilized demonstrated in missing anomaly near above the T_C. The substituted electronic system is more sensitive to relative Er- and Co-sublattice distances proved by stronger pressure dependency up to ~ 1.5 GPa as for the parent $ErCo_2$ system (see Fig. 6.17).
3. The induced Co-magnetic moment decreases linearly with the applied pressure (up to studied 1GPa). The Si substitution causes changes in density of states (a *p-d* hybridisation plays a significant role) resulting in a stabilizer moment and so pressure influence is smaller than in the parent system.
4. On the other hand, the Si substitution has a negative influence on the Co-clusters formation. Although the Co-Co exchange interactions should decrease due to increased relative Co distances it is proved that arisen *p-d* hybridisation is stronger resulting in stronger Co-Co-exchange interactions and decrease in flipping temperature. From the pressure experiments follows this hybridised system is more

sensitive to pressure application as the original one.

To confirm and further refine the proposed scenario XMCD experiments with appropriate pressure cells are strongly desirable.
In addition, we have pursued a comparative study of the influence of hydrostatic and uniaxial (along the easy magnetization direction) pressure, respectively, on T_C and Er magnetic moment in the $ErAl_2$ single crystal. To explain the obtained changes of the Er magnetic moment with uniaxial pressure a scenario considering variation of crystal field parameters has been proposed.

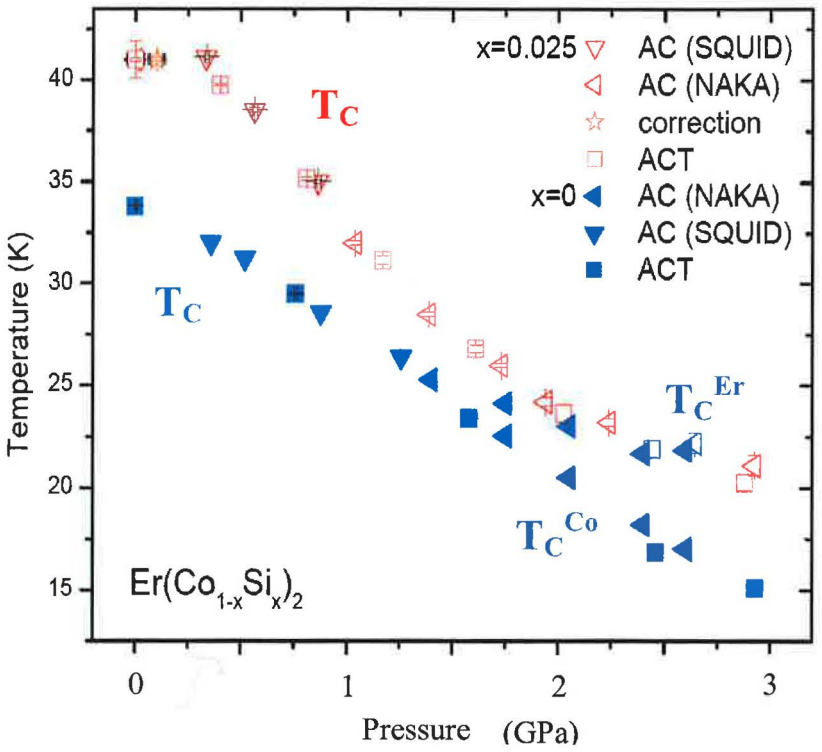

Figure 6.17 Summarizing phase diagram T_C vs. P for $ErCo_2$ and $Er(Co_{0.975}Si_{0.025})_2$.

Appendix A

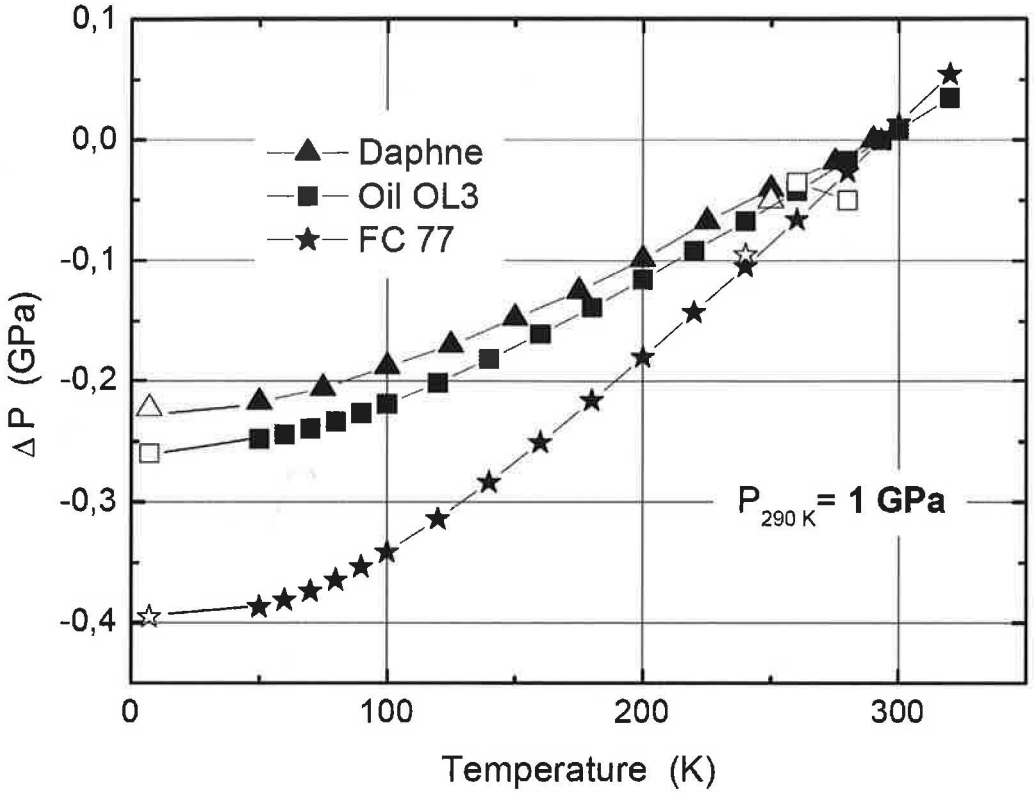

Figure A.1 Comparisson of temperature induced pressure variations in clamped cells for different transmitting media.

Reference

[1] N. W. Ashcroft and N. D. Mermin, *Solid State Physics*, Thomson Learning, Inc., 1976.

[2] S. Blundell, *Magnetism in Condesed Matter*, Oxford University Press, 2001.

[3] C. Lacroix, *Introduction to Magnetism* in *Magnetism: A Synchrotron Radiation Approach*, Springer Berlin / Heidelberg, 2006.

[4] P. Mohn, *Itinerant Electron Systems: Magnetism (Ferromagnetism)* in *Encyclopaedia of Condensed Matter Physics*. (Ed. F. Bassani, G. L. Liedl and P. Wyder), Elsevier Science Ltd., 2001.

[5] D. Givord, *Introduction to Magnetism and Magnetic Materials* in *Magnetism and Synchrotron Radiation*, Springer Berlin / Heidelberg, 2001.

[6] K. H. J. Bushow and F. R. de Boer, *Physics of Magnetism and Magnetic Materials*, Kluwer Academic Publishers, 2004.

[7] D. Gignoux, F. Givord, R. Lemaire and F. Tasset, *Onset of Ferromagnetism and Spin Fluctuations in Rare-Earth (Or Actinide)-3D Compounds,* Journal of the Less-Common Metals 94, 1-15 (1983).

[8] E. P. Wohlfarth and P. Rhodes, *Collective Electron Metamagnetism*, Philosophical Magazine 7, 1817-& (1962).

[9] H. Ibach and H. Luth, *Solid-State Physics - An Introduction to Theory and Experiment*, Springer-Verlag, 1991.

[10] P. Mohn and S. Khmelevskyi, *Spin Fluctuations in Itinerant Electron Systems* in *Band-Ferromagnetism*. Springer Berlin / Heidelberg, 2008.

[11] T. Moriya, *Nuclear Magnetic Relaxation in Antiferromagnetics*, Progress of Theoretical Physics 16, 23-44 (1956).

[12] K. K. Murata and S. Doniach, *Theory of Magnetic Fluctuations in Itinerant Ferromagnets*. Physical Review Letters 29, 285-& (1972).

[13] J. Singleton, *Band Theory and Electronic Properties of Solids*, Oxford University Press, 2001.

[14] J. Kamarád, Unpublished Work

[15] Z. Arnold, *High pressure in basic and material science*, 2009, Unpublished Work

[16] S. K. Sikka and V. Vijayakumar, *Electronic structure changes at high pressures* in *Electronic Band Structure and Its Applications*, Springer Berlin / Heidelberg, 1987.

[17] J. Kamarád, *Magnetic Systems: External Pressure - induced Phenomena* in *Encyclopaedia of Condensed Matter Physics,* (Ed. F. Bassani, G. L. Liedl and P. Wyder), Elsevier Science Ltd., 2001.

[18] D. Konopka and W. Zarek, *Crystallographic and Magnetic Investigations of the Intermetallic System Erco2-Eral2*, Journal of the Less-Common Metals 81, 5-13 (1981).

[19] A. Iandelli and A. Palenzona, *Chapter 13 Crystal chemistry of intermetallic compounds* in *Handbook on the Physics and Chemistry of Rare Earths Alloys and Intermetallics* (Ed. A. G. Karl), Elsevier, 1979.

[20] T. D. Cuong, L. Havela, V. Sechovsky, A. V. Andreev, Z. Arnold, J. Kamarad and N. H. Duc, *Magnetism and related phenomena in RE(Co1-xSix)(2) compounds,* Journal of Alloys and Compounds 262, 141-146 (1997).

[21] T. D. Cuong, L. Havela, V. Sechovsky, A. V. Andreev, Z. Arnold, J. Kamarad and N. H. Duc, *Band metamagnetism and related phenomena in Er(Co1-xSix)(2)*, Journal of Applied Physics 81, 4221-4223 (1997).

[22] T. D. Cuong, N. H. Duc, P. E. Brommer, Z. Arnold, J. Kamarad and V. Sechovsky, *Co magnetism and related phenomena in the Er(Co1-xSix)(2) compound,*. Journal of Magnetism and Magnetic Materials 182, 143-151 (1998).

[23] T. Inoue, S. G. Sankar, R. S. Craig, W. E. Wallace and K. A. Gschneidner, *Low-Temperature Heat-Capacities and Thermal-Properties of Dyal2, Eral2 and Lual2*, Journal of Physics and Chemistry of Solids 38, 487-497 (1977).

[24] E. M. Levin, V. K. Pecharsky and K. A. Gschneidner, *Real and imaginary components of the alternating current magnetic susceptibility of RAl2 (R=Gd, Dy, and Er) in the ferromagnetic region*, Journal of Applied Physics 90, 6255-6262 (2001).

[25] J. X. Boucherle, A. Gregory, J. Schweizer and G. Will, *Magnetic Form-Factor of Eral2*, Physica B 156, 734-736 (1989).

[26] H. G. Purwins, *Magnetization Curves of Eral2 Single Crystals and Recoilles Gamma Resonance at Er-166 in Er1-Xgdxal2*, Physics Letters A A 31, 523-& (1970).

[27] H. G. Purwins, E. Walker, B. Barbara, M. F. Rossignol and A. Furrer, *Single-Crystal Magnetization of Eral-2 and Interpretation in Terms of Crystalline Field*, Journal of Physics C-Solid State Physics 9, 1025-1030 (1976).

[28] J. C. P. Campoy, E. J. R. Plaza, A. A. Coelho and S. Gama, *Magnetoresistivity as a probe to the field-induced change of magnetic entropy in RAl2 compounds (R=Pr,Nd,Tb,Dy,Ho,Er)*, Physical Review B 74, (2006).

[29] C. Giorgetti, E. Dartyge, F. Baudelet and R. M. Galera, *XMCD at the L-II,L-III edges of er in ErMn2, ErFe2, ErCo2, ErNi2, and ErAl2 laves phases and in Er-2(SO4)(3), 8H(2)0*, Physical Review B 70, (2004).

[30] F. Garcia, H. dos Santos, M. R. Soares, A. Y. Takeuchi and S. F. da Cunha, *Recovery of ErCo2 Fermi level by substitution of Co by Ni and Fe*, Journal of Applied Physics 83, 6969-6970 (1998).

[31] F. Garcia, M. R. Soares, A. Y. Takeuchi and S. F. da Cunha, *Changeover in the order of the magnetic phase transition in the intermetallic compounds (Er1-xTbx)Co-2*, Journal of Alloys and Compounds 279, 117-122 (1998).

[32] N. V. Baranov and A. I. Kozlov, *Magnetoresistance in Erco2 and Hoco2 Single-Crystals*, Journal of Alloys and Compounds 190, 83-86 (1992).

[33] T. Goto, K. Fukamichi, T. Sakakibara and H. Komatsu, *Itinerant Electron Metamagnetism in Yco2*, Solid State Communications 72, 945-947 (1989).

[34] T. Goto, H. A. Katori, T. Sakakibara, H. Mitamura, K. Fukamichi and K. Murata, *Itinerant-Electron Metamagnetism and Related Phenomena in Co-Based Intermetallic Compounds (Invited),* Journal of Applied Physics 76, 6682-6687 (1994).

[35] S. Khmelevskyi and P. Mohn, *The order of the magnetic phase transitions in RCo2 (R = rare earth) intermetallic compounds*, Journal of Physics-Condensed Matter 12, 9453-9464 (2000).

[36] R. Hauser, E. Bauer, E. Gratz, H. Muller, M. Rotter, H. Michor, G. Hilscher, A. S. Markosyan, K. Kamishima and T. Goto, *Decoupling of the magnetic ordering of the rare-earth and the Co sublattice in Er1-xYxCo2 compounds driven by substitution or pressure*, Physical Review B 61, 1198-1210 (2000).

[37] D. Bloch, D. M. Edwards, M. Shimizu and J. Voiron, *1St Order Transitions in Aco2 Compounds*, Journal of Physics F-Metal Physics 5, 1217-1226 (1975).

[38] J. Inoue and M. Shimizu, *1St-Order and 2Nd-Order Magnetic Phase-Transitions in (R-Y)Co2 and R(Co-Al)2 (R = Heavy Rare-Earth Element) Compounds*, Journal of Physics F-Metal Physics 18, 2487-2497 (1988).

[39] J. Inoue and M. Shimizu, *Volume Dependence of the 1St-Order Transition-Temperature for Rco2 Compounds*, Journal of Physics F-Metal Physics 12, 1811-1819 (1982).

[40] E. Gratz and A. S. Markosyan, *Physical properties of RCo2 Laves phases*, Journal of Physics-Condensed Matter 13, R385-R413 (2001).

[41] E. P. Wohlfarth and P. Rhodes, *Collective Electron Metamagnetism*, Philosophical Magazine 7, 1817-& (1962).

[42] O. Syshchenko, T. Fujita, V. Sechovsky, M. Divis and H. Fujii, *Magnetism in RECo2 compounds under high pressure*, Journal of Magnetism and Magnetic Materials 226, 1062-1067 (2001).

[43] N. H. Duc, T. D. Hien, R. Z. Levitin, A. S. Markosyan, P. E. Brommer and J. J. M. Franse, *The Magnetic Phase-Transitions in R(Co, Al)2 Compounds (R Dy, Ho, Er)*, Physica B 176, 232-238 (1992).

[44] O. Syshchenko, T. Fujita, V. Sechovsky, M. Divis and H. Fujii, *Magnetism in HoCo2 and ErCo2 under high pressure,* Journal of Alloys and Compounds 317, 438-442 (2001).

[45] O. Syshchenko, T. Fujita, V. Sechovsky, M. Divis and H. Fujii, *Magnetism in ErCo2 under high pressure*, Physical Review B 63, (2001).

[46] H. Imai, H. Wada and M. Shiga, *Calorimetric Study on Magnetism of Erco2*, Journal of Magnetism and Magnetic Materials 140, 835-836 (1995).

[47] D. Vasylyev, J. Prokleska, J. Sebek and V. Sechovsky, *Thermal properties of Er(Co1-xSix)(2) compounds*, Journal of Alloys and Compounds 394, 96-100 (2005).

[48] H. Wada, Y. Tanabe, M. Shiga, H. Sugawara and H. Sato, *Magnetocaloric effects of Laves phase Er(Co1-xNix)(2) compounds*, Journal of Alloys and Compounds 316, 245-249 (2001).

[49] M. R. Soares, A. Y. Takeuchi, F. Garcia, S. F. da Cunha and M. El Massalami, Magnetic phase diagram of the intermetallic series Er(Co1-xNix)(2). Journal of Magnetism and Magnetic Materials 202, 473-479 (1999).

[50] T. D. Cuong, L. Havela, V. Sechovsky, A. V. Andreev, Z. Arnold, J. Kamarad and N. H. Duc, *Band metamagnetism and related phenomena in Er(Co1-xSix)(2)*, Journal of Applied Physics 81, 4221-4223 (1997).

[51] T. D. Cuong, N. H. Duc, P. E. Brommer, Z. Arnold, J. Kamarad and V. Sechovsky, *Co magnetism and related phenomena in the Er(Co1-xSix)(2) compounds*, Journal of Magnetism and Magnetic Materials 182, 143-151 (1998).

[52] S. Danis, P. Javorsky, D. Rafaja and V. Sechovsky, *Low-temperature transport and crystallographic studies of Er(Co1-xSix)(2) and Er(Co1-xGex)(2)*, Journal of Alloys and Compounds 345, II (2002).

[53] N. H. Duc, T. D. Hien, P. E. Brommer and J. J. M. Franse, *Magnetic-Properties of the Er(Co1-Xcux)2 and Y(Co1-Xcux)2 Compounds*, Physica B & C 149, 352-360 (1988).

[54] N. H. Duc, T. D. Hien, P. E. Brommer and J. J. M. Franse, *Electronic and Magnetic-Properties of Erxy1-Xco2 Compounds,* Journal of Physics F-Metal Physics 18, 275-294 (1988).

[55] N. H. Duc, T. D. Hien, P. P. Mai and P. E. Brommer, *Role of the Rare-Earth Atoms Affecting the Spin Fluctuation Scattering in the (Re, Y)Co2 Compounds*, Physica B 172, 399-404 (1991).

[56] J. Woo, Y. Jo, H. C. Kim, A. Pirogov, J. G. Park, H. C. Ri, A. Podlesnyak, J. Schefer, T. Strassle and A. Teplykh, *Studies of single crystal ErCo2 under pressure and magnetic field*, Physica B-Condensed Matter 329, 653-654 (2003).

[57] F. Garcia, M. R. Soares and A. Y. Takeuchi, *Spin fluctuation in RCo2 compounds*. Journal of Magnetism and Magnetic Materials 226, 1197-1199 (2001).

[58] J. Prokleska, J. Vejpravova, D. Vasylyev and V. Sechovsky, *Magnetism of Er(Co-1-X-x(x))(2) compounds: effects on structure and electronic properties.* Journal of Alloys and Compounds 383, 122-125 (2004).

[59] R. M. Moon, W. C. Koehler and J. Farrell, *Magnetic Structure of Rare-Earth-Cobalt (Rco2) Intermetallic Compounds*. Journal of Applied Physics 36, 978-& (1965).

[60] J. Herrero-Albillos, F. Bartolome, L. M. Garcia, J. Campo, A. T. Young, T. Funk and G. J. Cuello, *Ferrimagnetic correlations in paramagnetic ErCo2*. Journal of Magnetism and Magnetic Materials 310, 1645-1647 (2007).

[61] J. Herrero-Albillos, L. M. Garcia, F. Bartolome, A. T. Young and T. Funk, *Experimental evidence of intrinsic Co magnetic moment in paramagnetic ErCo2.* Journal of Magnetism and Magnetic Materials 316, E442-E445 (2007).

[62] J. Herrero-Albillos, F. Bartolome, L. M. Garcia, A. T. Young, T. Funk, J. Campo and G. J. Cuello, *Observation of a different magnetic disorder in ErCo2*. Physical Review B 76, (2007).

[63] U. Atzmony and G. Dublon, *Directions of Easy Magnetization in Laves Rco2 Compounds*. Physica B & C 86, 167-168 (1977).

[64] M. I. Bartashevich, H. A. Katori, T. Goto, H. Wada, T. Maeda, T. Mori and M. Shiga, *Collapse of the itinerant Co moment in Er1-xLuxCo2 by the application of high magnetic fields.* Physica B 229, 315-320 (1997).

[65] H. Yamada, *Effect of Pressure on the Metamagnetic Transition in An Itinerant-Electron System.* Physica B 201, 151-154 (1994).

[66] H. Yamada, *Pressure Effect of Metamagnetic Transition in Yco2 and Luco2.* Physica B 211, 161-164 (1995).

[67] H. Yamada, *Pressure Effect in An Itinerant-Electron Metamagnet at Finite-Temperature.* Journal of Magnetism and Magnetic Materials 139, 162-170 (1995).

[68] N. Ishimatsu, S. Miyamoto, H. Maruyama, J. Chaboy, M. A. Laguna-Marco and N. Kawamura, *Experimental evidence of pressure-induced suppression of the cobalt magnetic moment in ErCo2*. Physical Review B 75, (2007).

[69] X. B. Liu and Z. Altounian, *Co magnetism and the order of the magnetic transition in Er1-xGdxCo2 Laves phases*. Journal of Applied Physics 99, (2006).

[70] N. A. de Oliveira, *Magnetocaloric effect under applied pressure and the barocaloric effect in the compounds RCo2 (R = Er, Ho and Dy)*. Journal of Physics-Condensed Matter 20, (2008).

[71] X. B. Liu and Z. Altounian, *Magnetic states and magnetic transitions in RCo2 Laves phases*. Journal of Physics-Condensed Matter 18, 5503-5516 (2006).

[72] J. Vejpravová. *Impurities in rare earth metallic system: from super-purified metals to heavy fermion superconductors*. Dissertation, 2007

[73] Fullprof. Computer Program, 2009.

[74] Quantum Design. MPMS - Magnetic Property Measurement System, User's Manual. 2004.

[75] Quantum Design. PPMS - Physical Property Measurement System, User's Manual. 2004.

[76] Squid Magnetometer. http://hyperphysics.phy-astr.gsu.edu/Hbase/solids/squid.html#c1

[77] J. Clarke, *SQUIDs: The Instrument in Encyclopaedia of Condensed Matter Physics,* Elsevier Science Ltd., 2001.

[78] J. Brož, *Základy fysikálních mìøení*, Státní pedagogické nakladatelství, 1967

[79] J. Prchal, *Closed Cycle Refrigerator principle*, Personal Communication, 2009

[80] J. Kamarád. *Hydrostatic clamped pressure cell for ACMS measurements in SQUID magnetometer*. User's manual, 2007

[81] M. Eremets, *High Pressure Experimenzal Methods*, Oxford University Press, 1996.

[82] J. Kamarad, M. Mihalik, V. Sechovsky and Z. Arnold, *Miniature uniaxial pressure cells for magnetic measurements*. High Pressure Research 28, 633-636 (2008).

[83] A. Arrott, *Criterion for Ferromagnetism from Observations of Magnetic Isotherms*. Physical Review 108, 1394-1396 (1957).

[84] T. D. Cuong. *Magnetism and related properties of RECo2 compounds: Co - dilution*. Dissertation, 1998

[85] X. B. Liu and Z. Altounian, *Magnetocaloric effect in co-rich Er(Co1-xFex)(2) laves phase.* Journal of Applied Physics 103, (2008).

[86] N. H. Duc and T. K. Oanh, *Magnetic and electrical properties of the Ho(Co,Si)(2) compounds*. Journal of Physics-Condensed Matter 9, 1585-1598 (1997).

[87] N. H. Duc, V. Sechovsky, D. T. Hung and N. H. Kimngan, *Influence of Al-Atoms on the Spin Fluctuation Scattering in R(Co, Al)2 Compounds*. Physica B 179, 111-116 (1992).

[88] K. Murata, K. Fukamichi, T. Goto, K. Suzuki and T. Sakakibara, *The Lattice-Constant and Itinerant-Electron Metamagnetic Transition in Laves-Phase Pseudo-Binary Lu(Co1-Xsix)2 Compounds*. Journal of Physics-Condensed Matter 6, 6659-6666 (1994).

[89] N. H. Duc, *Magnetic and electrical properties of the R(Co, Si)(2) compounds (R=Gd, Tb, dy) with invariable crystal unit cell parameters*. Journal of Magnetism and Magnetic Materials 152, 219-225 (1996).

[90] M. Aoki and H. Yamada, *Electronic-Structure and Magnetism of C15-Type Laves Phase-Compounds Y(Co, Al)2 and Y(Co, Si)2*. Physica B 177, 259-261 (1992).

[91] Y. Oner, E. Alveroglu and O. Kamer, *Low-field magnetic-properties of ErCo2 intermetallic compound.* Journal of Alloys and Compounds 424, 60-66 (2006).

[92] J. Prokleška. *Magnetoelastické jevy ve slouèeninách Er(Co,X)2, X=p-element.* Diploma Thesis, 2003.

[93] R. Hauser, E. Bauer and E. Gratz, *Pressure-dependent electrical resistivity of RCo2 compounds (R = rare earth)*. Physical Review B 57, 2904-2914 (1998).